A Common Origin of the H_0 and S_8 Cosmological Tensions and a Resolution within a Modified ΛCDM Framework

Dimitris M. Christodoulou *, Demosthenes Kazanas, Silas G. T. Laycock

Posted Date: 14 January 2026

doi: 10.20944/preprints202601.1031.v1

Keywords: cosmological constant; cosmology; dark energy; Friedmann equations; Hubble constant

Article

A Common Origin of the H_0 and S_8 Cosmological Tensions and a Resolution within a Modified ΛCDM Framework

Dimitris M. Christodoulou [1,*], Demosthenes Kazanas [2] and Silas G. T. Laycock [3]

[1] Department of Mathematical Sciences, DePaul University, Chicago, IL 60614, USA
[2] Astrophysics Science Division, Code 663, NASA Goddard Space Flight Center, Greenbelt, MD 20771, USA
[3] Lowell Center for Space Science and Technology, University of Massachusetts Lowell, Lowell, MA, 01854, USA
* Correspondence: dchris32@depaul.edu or dimitris_christodoulou@uml.edu

Abstract

The two most severe cosmological tensions in the Hubble constant H_0 and the matter clustering amplitude S_8 have the same relative discrepancy of 8.3%, which suggests that they may have a common origin. Modifications of gravity and exotic dark fields with numerous free parameters introduced in the Einstein field equations often struggle to simultaneously alleviate both tensions; thus, we need to look for a common cause within the standard ΛCDM framework. At the same time, linear perturbation analyses of matter in the expanding ΛCDM universe have always neglected the impact of comoving peculiar velocities $\mathbf{v}$ (generally thought to be a second-order effect), the same velocities that in physical space cannot be fully accounted for in the observed late-time universe when the cosmic distance ladder is used to determine the local value of H_0. We have reworked the linear density perturbation equations in the conformal Newtonian gauge (sub-horizon limit) by introducing an additional drag force per unit mass $-\Gamma(t)\mathbf{v}$ in the Euler equation with $\Gamma \equiv \gamma(2H)$, where $\gamma \ll 1$ is a positive dimensionless constant and $2H(t)$ is the time-dependent Hubble friction. We find that a damping parameter of $\gamma = 0.083$ is sufficient to resolve the S_8 tension by suppressing the growth of structure at low redshifts, starting at $z_\star \simeq 3.5$–6.5 to achieve $S_8 \simeq 0.78$–0.76, respectively. Furthermore, we argue that the physical source causing this additional friction (a tidal field generated by nonlinear structures in the late-time universe) is also responsible for a systematic error in the local determinations of H_0: the inability to subtract peculiar tidal velocities along the lines of sight when determining the Hubble flow via the cosmic distance ladder. Finally, the dual action of the tidal field on the expanding background—reducing both the matter and the dark-energy sources of the squared Hubble rate H^2, thereby holding back the cosmic acceleration $\ddot{a}$—is of fundamental importance in resolving cosmological tensions and can also substantially alleviate the density coincidence problem.

Keywords: cosmological constant; cosmology; dark energy; Friedmann equations; Hubble constant

1. Introduction

1.1. Standard ΛCDM Model

The standard ΛCDM cosmological model has enjoyed remarkable success over the past two decades, providing a consistent framework that explains a vast array of observations, from the temperature anisotropies of the cosmic microwave background (CMB) to the large-scale distribution of galaxies [1,2]. Based on a spatially flat universe dominated by cold dark matter (CDM) and a cosmological constant Λ [3–6], the ΛCDM model is specified by six parameters, which have been constrained with sub-percent precision by the Planck satellite mission [1]. On the other hand, the cosmological constant itself presents one of the most profound theoretical challenges in physics today, known by its components as the cosmological constant problem (CCP) and the density coincidence problem (DCP), respectively [7,8]:

 doi:10.20944/preprints202601.1031.v1

(1) CCP: Quantum field theory predicts a vacuum energy density vastly greater than the observed value by more than 120 orders of magnitude [9,10].
(2) DCP: The effective density corresponding to Λ and the density of matter are comparable at the present epoch, requiring highly contrived initial conditions to reach this universal state [11,12].

These fundamental puzzles motivate a search for cosmological mechanisms that can drive the late-time acceleration of the universe without relying on extreme fine-tuning assumptions.

1.2. Major Cosmological Tensions

As observational precision has improved over the years, some statistically significant cracks have appeared in the ΛCDM foundation. In particular, two major discrepancies have persisted and intensified, suggesting the presence of systematic errors in diverse observational datasets and the need for more physics unaccounted for in ΛCDM—or, alternatively, the necessity to modify gravity at large scales by including exotic new physics and more dark, undetected fields in cosmological theories [13–15].

The first and most prominent discrepancy is the "Hubble tension," concerning the value of the current expansion rate H_0. Estimates of H_0 inferred from early-universe physics (CMB) assuming ΛCDM consistently yield lower values of $H_0 \simeq 67.4$ km s^{-1} Mpc^{-1} [1]. In stark contrast, local late-universe measurements using the cosmic distance ladder (CDL) consistently favor a higher value of $H_0 \simeq 73.0$ km s^{-1} Mpc^{-1} [15–17]. The statistical significance of this discrepancy has reached the 5σ level, rendering it impossible to dismiss as a mere statistical fluctuation [16].

The second major discrepancy is the "S_8 tension," which involves the clumpiness of baryonic matter observed in the late universe. The parameter S_8 quantifies the amplitude of density fluctuations. Predictions based on Planck CMB data project a relatively high degree of clustering ($S_8 \simeq 0.834$) [1]. Conversely, direct measurements of late-time large-scale structure (LSS) from weak gravitational lensing and galaxy clustering surveys, such as the Kilo-Degree Survey (KiDS) [18] and the Dark Energy Survey (DES) [19], consistently measure a lower amplitude ($S_8 \approx 0.76$–0.78). The growth history of the LSS provides a powerful test of the background evolution [20]. While the statistical significance of this tension (~2–3σ) is lower than that of H_0, its persistence across independent low-redshift probes suggests a genuine physical anomaly: our universe is smoother than what ΛCDM predicts.

1.3. A Remarkable Coincidence and a New Path Forward

In this work, we highlight first a striking coincidence that has largely gone unnoticed: the relative difference of the two major tensions is virtually identical:

(a) The relative discrepancy in H_0 [1,15,16] is

$$(73.0 - 67.4)/67.4 \;=\; 8.3\%\,.$$

(b) The relative discrepancy in S_8 [1,15,18] is

$$(0.834 - 0.77)/0.77 \;=\; 8.3\%\,.$$

We argue that this concordance in relative discrepancies is not coincidental. Rather, it points toward a single underlying physical mechanism responsible for both cosmological tensions. The missing physics ought to be capable of simultaneously (i) suppressing the predicted LSS growth rates by about 8.3%, and (ii) resolving the 8.3% overestimate of H_0 that currently appears in the local CDL measurements.

While numerous extensions to ΛCDM have been proposed—ranging from early dark energy [21] to modified gravity theories [22] and models involving coupled dark sectors [23]—these solutions typically introduce complex exotic fields with multiple free parameters, a generally undesirable trade-off. Furthermore, such fields often struggle to resolve both tensions simultaneously; mechanisms that

 doi:10.20944/preprints202601.1031.v1

alleviate the H_0 tension frequently exacerbate the S_8 tension [24,25]. For these reasons, we choose to improve ΛCDM without invoking new exotic physics.

To this end, we revisit the standard model, searching for minimal adjustments that could simultaneously account for both of the above ~ 8.3% tensions, and we consider linear density perturbations within this framework [10,26]. Standard treatments typically assume a perfect cosmic fluid of collisionless dust, in which perturbations grow by gravitational instability [27], while gravitational attraction is counteracted to a degree by the Hubble flow. The fluid peculiar velocities affecting the linear density perturbations have traditionally been neglected in the linearized Euler equation (as a nonlinear effect [28,29]), even in the low-redshift universe when the cosmic deceleration has significantly diminished. But peculiar velocities are also the source of noise and uncertainty that complicate the determination of recession velocities in the local CDL measurements [30]. Thus, if tidal interactions from exterior nonlinear structures introduce radial velocities into the linear regime at late times [28], the resulting drag forces could systematically distort our interpretations of both key local rates, the background expansion rate H_0 and the LSS growth rate S_8.

Based on the above reasoning, we test a modification of the linear perturbation equation in the sub-horizon limit of the conformal Newtonian gauge by introducing a first-order drag force proportional to the amplitude of the peculiar velocity itself. This drag acts as an additional friction that suppresses somewhat the growth of structure. In this paper, we demonstrate that a drag amplitude $\gamma \lesssim 8.3\%$ of $2H(t)$ at low redshifts, along with the Hubble friction $2H(t)$, is sufficient to suppress the LSS growth rate and resolve the S_8 tension. Furthermore, we argue that the same mechanism may account for the apparent excess in the locally measured H_0 values, thereby offering a unified "γΛCDM" resolution of the two major tensions in modern ΛCDM cosmology and other identified discrepancies [15].

1.4. Outline

The remainder of the paper is organized as follows:

- In Section 2, we introduce an additional drag term to the Euler equation and perform the linear perturbation analysis in the conformal Newtonian gauge within the FLRW background.
- In Section 3, we determine typical values of S_8 in our modified γΛCDM framework and we examine whether the S_8 tension can be resolved by accounting for the added time-dependent friction ($\gamma \lesssim 8.3\%$ of $2H$) induced by drag forces due to an exterior tidal field (statistically isotropized, but with a nonzero mean value).
- In Section 4, we examine how this kinematic enhancement of the Hubble expansion modifies the background dynamics of the standard ΛCDM model to linear order in $\gamma \ll 1$.
- In Section 5, we develop a simplified 1-D radial line-of-sight model and estimate the $O(\gamma)$ net tidal acceleration acting on a target galaxy, as well as the implied magnitude of γ.
- In Section 6, we summarize our conclusions.
- In Appendix A, we show that the modifications introduced to the kinematics and the dynamics of the Hubble flow are consistent with one another.

2. Linear Perturbations with a Time-Dependent Drag Force

We formulate the linear scalar perturbation equations for a FLRW universe with dust, a cosmological constant, and a time-dependent drag force due to a peculiar velocity field. The analysis is performed in comoving spatial coordinates $\mathbf{x}$ and cosmic time t. The background dynamics follows the standard spatially flat ΛCDM model, while the perturbations obey modified Euler dynamics due to the additional friction term.

2.1. Initial Assumptions and Kinematic Framework

We consider a spatially flat FLRW spacetime with line element

$$ds^2 = -c^2dt^2 + a^2(t)\,d\mathbf{x}^2\,, \tag{1}$$

 doi:10.20944/preprints202601.1031.v1

where $a(t)$ is the scale factor and c is the speed of light in vacuum. The background expansion rate is given by the Hubble function

$$H(t) \equiv \frac{\dot{a}(t)}{a(t)}. \tag{2}$$

The matter sector is assumed to be a pressureless perfect fluid (dust) with background density $\rho(t)$ satisfying the continuity equation

$$\dot{\rho} + 3H\rho = 0. \tag{3}$$

The background evolution of a, H, and ρ is governed by the usual Friedmann equations (FEs) with a cosmological constant Λ and a gravitational constant G, viz.

$$H^2 = \frac{\Lambda c^2}{3} + \frac{8\pi G\rho}{3}, \tag{4}$$

$$\frac{\ddot{a}}{a} = \frac{\Lambda c^2}{3} - \frac{4\pi G\rho}{3} \tag{5}$$

Combining the FEs and using the identity $\ddot{a}/a = \dot{H} + H^2$, we obtain the Raychaudhuri–Landau equation for $H(t)$ [31], viz.

$$2\dot{H} + 3H^2 = \Lambda c^2. \tag{6}$$

This equation relates the cosmic acceleration $\dot{H}$ with the Hubble expansion rate H and the cosmological constant Λ.

2.2. Linearized Perturbation Equations

2.2.1. Preliminaries

In the FLRW background, we introduce small perturbations to linear order. The density field is decomposed as

$$\rho(t,\mathbf{x}) = \rho(t)[1 + \delta(t,\mathbf{x})], \quad |\delta| \ll 1, \tag{7}$$

where $\delta(t,\mathbf{x})$ is the density contrast in comoving coordinates $\mathbf{x}$.

The gravitational potential $\Phi(t,\mathbf{x})$, which encodes the perturbation of the metric sourced by these density fluctuations, represents the scalar metric perturbation in the conformal Newtonian gauge. In the Newtonian (sub-horizon) limit, where time derivatives of the metric potentials are negligible and spatial gradients dominate, the linearized fluid equations reduce to their familiar comoving Newtonian forms. In this regime, Φ satisfies the standard Poisson equation relating the gravitational potential to the comoving density perturbations [10,26].

The proper velocity of the fluid relative to an observer at the origin $\mathbf{r} = \mathbf{0}$ is defined as $\mathbf{u}(t,\mathbf{x}) \equiv d\mathbf{r}/dt$. We decompose $\mathbf{u}$ into the Hubble flow and the peculiar velocity $\mathbf{v}(t,\mathbf{x})$ as

$$\mathbf{u}(t,\mathbf{x}) = H(t)\mathbf{r} + \mathbf{v}(t,\mathbf{x}), \tag{8}$$

where $H(t)$ is the Hubble rate and $|\mathbf{v}| \ll H\mathbf{r}$. The peculiar velocity measures departures from the pure Hubble flow and is related to the comoving coordinates $\mathbf{x} = \mathbf{r}/a(t)$ by

$$\mathbf{v}(t,\mathbf{x}) = a(t)\frac{d\mathbf{x}}{dt}. \tag{9}$$

The perturbed Euler equation is modified by the introduction of a time-dependent drag force per unit mass $\mathbf{a}_{\rm drag}$. When expressed in terms of the peculiar velocity, this physical deceleration is assumed to take the form

$$\mathbf{a}_{\rm drag}(t,\mathbf{x}) = -\Gamma(t)\,\mathbf{v}(t,\mathbf{x}), \tag{10}$$

 doi:10.20944/preprints202601.1031.v1

where $\Gamma(t)$ is an arbitrary non-negative function of cosmic time with the dimension of frequency. This ensures that the friction enters the linear growth equation as an additive damping term.

2.2.2. First-Order Equations

To first order in the quantities δ, $\mathbf{v}$, and Φ, the continuity, Euler, and Poisson equations for a fluid of dust subject to the time-dependent drag deceleration (10), respectively, are

$$\dot{\delta} + \frac{1}{a}\nabla \cdot \mathbf{v} = 0, \tag{11}$$

$$\dot{\mathbf{v}} + H\mathbf{v} = -\frac{1}{a}\nabla\Phi - \Gamma(t)\mathbf{v}, \tag{12}$$

$$\frac{1}{a^2}\nabla^2\Phi = (4\pi G\rho)\delta. \tag{13}$$

This system of equations is closed and can be reduced to a single differential equation for the linear growth of density perturbations $\delta(t)$: We define the comoving divergence of peculiar velocities

$$\theta \equiv \frac{1}{a}\nabla \cdot \mathbf{v}, \tag{14}$$

which represents the rate at which the fluid is fluctuating in comoving space. The continuity equation (11) then becomes

$$\theta = -\dot{\delta}. \tag{15}$$

Next, taking the comoving divergence of the Euler equation (12), we obtain the equation

$$\dot{\theta} + 2H\theta = -\frac{1}{a^2}\nabla^2\Phi - \Gamma(t)\,\theta, \tag{16}$$

and substituting $\nabla^2\Phi/a^2$ from the Poisson equation (13) and θ from equation (15), we obtain the final form

$$\ddot{\delta} + (2H + \Gamma)\,\dot{\delta} - (4\pi G\rho)\,\delta = 0. \tag{17}$$

Equation (17) is an ordinary differential equation (ODE) that governs the cosmic evolution of a linear density Fourier mode $\delta_{\mathbf{k}}(t)$ with comoving wavenumber $\mathbf{k}$. Because the perfect fluid is assumed to be dust, the evolution of $\delta_{\mathbf{k}}(t)$ becomes independent of $\mathbf{k}$ on sub-horizon scales. In this sense, this equation generalizes the standard ΛCDM growth equation by including the friction coefficient $\Gamma(t) > 0$. This term enhances the conventional Hubble friction and results in greater suppression of the growth of linear density perturbations relative to the growth in the standard ΛCDM model with $\Gamma = 0$.

2.3. Scaling the Friction Coefficient $\Gamma(t)$

In the subsequent analysis, we scale $\Gamma(t)$ to the expansion-induced Hubble friction with coefficient $2H(t)$. We adopt the convenient form

$$\Gamma = \gamma(2H), \tag{18}$$

where $\gamma > 0$ is a dimensionless constant parameterizing the strength of the drag forces relative to the usual Hubble damping term. This choice ensures that the added friction is naturally scaled to the universal expansion, thereby simplifying further investigations. It is however expected that $\gamma \ll 1$.

Substituting Equation (18) into Equation (17), we find that the evolution of the density contrast $\delta(t)$ satisfies the linear differential equation

$$\ddot{\delta} + 2H(1+\gamma)\,\dot{\delta} - (4\pi G\rho)\,\delta = 0. \tag{19}$$

Naturally, for $\gamma = 0$, we recover the standard ΛCDM linear growth equation [10,26].

 doi:10.20944/preprints202601.1031.v1

The scaling constant γ in Equation (19) naturally provides a framework for addressing the observed S_8 tension, and it may also potentially alleviate the H_0 tension. In the following section, we determine the range of γ values that reconcile the predicted linear growth with current observational constraints on S_8 (≈ 0.76–0.78) [15].

3. Clustering Amplitudes and Growth Rates in ΛCDM with a Drag Force

3.1. Preliminaries

The linear growth factor (D) of structure is commonly defined in terms of the matter density contrast $\delta(a)$ [10,26], viz.

$$D(a) \equiv \frac{\delta(a)}{\delta(a_{\rm i})}, \tag{20}$$

where $a_{\rm i}$ is usually taken to be the scale factor at recombination (redshift $z_{\rm rec} \approx 1100$). For this reason, we introduce the scale factor as the independent variable in the ODE (19) for the matter density contrast, as shown in Sections 3.2 and 3.3 below. For the calculations, we also adopt

$$\ln a_{\rm i} = -7, \tag{21}$$

corresponding to $z_{\rm rec} = 1096$.

The RMS fluctuation amplitude $\sigma_8(\gamma = 0)$, linearly extrapolated to the present epoch and corresponding to the Planck-2018 ΛCDM normalization [1], is defined in terms of $D(a = 1; \gamma = 0)$ [10,26]. In our modified ΛCDM model, we correspondingly write $\sigma_8(\gamma)$, which we determine from the scaling relation

$$\sigma_8(\gamma) = \sigma_8(0)\left[\frac{D(a=1;\gamma)}{D(a=1;0)}\right], \tag{22}$$

where $\sigma_8(0) = 0.811 \pm 0.006$ [1].

The observational clustering parameter S_8 [1,32] is then determined by the relation

$$S_8(\gamma) = \sigma_8(\gamma)\sqrt{\frac{\Omega_{\rm m0}}{0.3}}, \tag{23}$$

where $\Omega_{\rm m0}$ is the matter density fraction at present time. Our modified model is essentially ΛCDM with enhanced friction, so we adopt the Planck-2018 value of $\Omega_{\rm m0} = 0.315 \pm 0.007$, for which Equation (23) reduces to

$$S_8(\gamma) = \frac{\sigma_8(\gamma)}{0.975\,900}, \tag{24}$$

precise to 6 significant digits.

In general, the matter density fraction varies with the scale factor and is defined as [10,26]

$$\Omega_{\rm m}(a) \equiv \frac{\rho(a)}{\rho_{\rm c}(a)}, \tag{25}$$

where $\rho(a) = \rho_0 a^{-3}$ is the background matter density, $\rho_0 = \rho(a = 1)$ at present ($a = 1$), and

$$\rho_{\rm c}(a) = \frac{3H(a)^2}{8\pi G}, \tag{26}$$

is the critical density in FLRW cosmology. We note that $\rho(a)$ refers to the total (CDM plus baryonic) matter component; on the linear scales of interest, the growth of structure $\delta(a)$ is dominated by dark matter with baryons acting as passive tracers of the overall gravitational potential wells.

It is convenient to introduce the dimensionless Hubble function $E(a) \equiv H(a)/H_0$, in terms of which the fraction $\Omega_{\rm m}(a)$ may be written as

$$\Omega_{\rm m}(a) = \frac{\Omega_{\rm m0}\, a^{-3}}{E(a)^2}, \tag{27}$$

 doi:10.20944/preprints202601.1031.v1

which satisfies $\Omega_{\rm m}(1) = \Omega_{\rm m0}$. The dimensionless Hubble function $E(a)$ is given by the well-known relation

$$E(a) \;=\; \sqrt{\Omega_{\rm m0}\, a^{-3} \,+\, \Omega_{\Lambda 0}}\,, \tag{28}$$

where $\Omega_{\Lambda 0} = 1 - \Omega_{\rm m0}$ is the vacuum energy fraction at present [1,10,26]. These quantities naturally appear in the gravitational source term of the linear growth equation derived below.

3.2. The ODE of the Matter Density Contrast $\delta(a)$

We change the independent variable in Equation (19) from cosmic time t to scale factor a [33] by using the identities

$$\frac{d}{dt} \;=\; aH\frac{d}{da} \qquad \text{and} \qquad \frac{d^2}{dt^2} \;=\; a^2H^2\frac{d^2}{da^2} \,+\, aH^2\!\left(1 + \frac{d\ln H}{d\ln a}\right)\frac{d}{da}\,. \tag{29}$$

Using primes to denote the derivatives with respect to a and replacing δ from Equation (20), we find that the linear growth equation is transformed to

$$D''(a) \,+\, \frac{1}{a}\left(2\gamma + 3 + \frac{d\ln H}{d\ln a}\right)D'(a) \,-\, \frac{3}{2}\frac{\Omega_{\rm m}(a)}{a^2}\,D(a) \;=\; 0\,. \tag{30}$$

In this ODE, a factor of 2γ effectively enhances the coefficient of Hubble friction ($3 + d\ln H/d\ln a$) and the gravitational source term depends on the mean universal density of matter at each instance.

For computational efficiency, it is convenient to also express the coefficient of friction in Equation (30) in terms of $\Omega_{\rm m}(a)$. The procedure simplifies the ODE considerably, viz.

$$D''(a) \,+\, \frac{1}{a}\left(2\gamma + 3 \,-\, \frac{3}{2}\Omega_{\rm m}(a)\right)D'(a) \,-\, \frac{3}{2}\frac{\Omega_{\rm m}(a)}{a^2}\,D(a) \;=\; 0\,, \tag{31}$$

where $\Omega_{\rm m}(a)$ can be computed from the compact expression

$$\Omega_{\rm m}(a) \;=\; \left(1 \,+\, \frac{\Omega_{\Lambda 0}}{\Omega_{\rm m0}}\,a^3\right)^{-1}\,, \tag{32}$$

which is derived by combining Equations (27) and (28). Here, the fiducial ratio $\Omega_{\Lambda 0}/\Omega_{\rm m0} = 2.174\,603$, precise to 7 significant digits [1].

3.3. Analytic Approximation for the Matter-Dominated Epoch

To gain analytic insight into the effect of the enhanced friction parameter γ, we consider an approximate solution of the growth Equation (31) in the matter-dominated regime. At early times ($a \ll 1$), Equation (32) implies that $\Omega_{\rm m}(a) \simeq 1$, so that Equation (31) reduces to a Cauchy-Euler ODE [34,35], viz.

$$D''(a) \,+\, \frac{1}{a}\left(2\gamma + \frac{3}{2}\right)D'(a) \,-\, \frac{3}{2a^2}\,D(a) \;=\; 0\,, \tag{33}$$

that admits power-law solutions of the form $D \propto a^p$, where p is a constant to be determined.

Substituting the power-law form into Equation (33), we find a quadratic equation for p, viz.

$$p^2 \,+\, \left(2\gamma + \frac{1}{2}\right)p \,-\, \frac{3}{2} \;=\; 0\,. \tag{34}$$

The power p_+ of the growing mode, expanded to linear order in $\gamma \ll 1$, is $p_+ = 1 - 4\gamma/5$. Since $D(a_{\rm i}) = 1$ (Equation (20)), the growing solution of the matter-dominated ODE (33) is

$$D(a) \;=\; \left(\frac{a}{a_{\rm i}}\right)^{1-4\gamma/5}\,. \tag{35}$$

 doi:10.20944/preprints202601.1031.v1

In standard ΛCDM where $\gamma = 0$, then $p_+ = 1$ and the growing mode is simply $D(a) = a/a_i$.

Extrapolating this solution to the present epoch ($a = 1$), we apply the results to Equation (22) for $\sigma_8(\gamma)$; using Equation (21), we find to linear order that

$$\mathcal{D}_1(\gamma) \equiv \frac{D(a=1;\gamma)}{D(a=1;0)} = (a_i)^{4\gamma/5} \simeq 1 - 5.6\,\gamma\,, \tag{36}$$

and that

$$\sigma_8(\gamma) \simeq \sigma_8(0)\,(1 - 5.6\,\gamma)\,. \tag{37}$$

The steep slope of −5.6 in $\sigma_8(\gamma)$ reflects the cumulative effect of a slightly enhanced Hubble friction (by $\gamma \ll 1$) over the long timescale from recombination ($a_i \simeq 10^{-3}$) to today. In a realistic ΛCDM background, this cumulative suppression of growth is expected to be mitigated because the drag forces are expected to become significant only at late times, when the causal nonlinear structures have been formed in the universe and $H(t)$ has significantly decreased with time.

Finally, a qualitative comparison with observations may be carried out using Equation (23) for $S_8(\gamma)$, with the important caveats that the analytic approximations above assume $\Omega_m \simeq 1$ and $\ln a_i = -7$. Within this framework, small values of the enhanced friction parameter of $\gamma \simeq 0.01$–0.015 reduce the ΛCDM-predicted clustering amplitude and alleviate the S_8 tension because the drag forces have been active at all times since recombination. In Section 3.4, we refine this rough estimate by numerically integrating the full growth Equation (31) for a range of γ-values and a range of initial conditions in a realistic ΛCDM background. In these computations, the critical redshift $z_\star$ at which drag forces first appear becomes a free parameter.

3.4. Numerical Solutions of the Growth Equation

To obtain precise estimates of the impact of the enhanced Hubble friction parameter γ on the growth of linear density perturbations for redshifts $z \le z_\star$, we integrate numerically the growth Equation (31). The integration of the growing solution begins in the early matter-dominated regime (standard ΛCDM with $\gamma = 0$ and $D = a/a_i$) at a scale factor corresponding to recombination, viz. $a_i = \exp(-7)$, where

$$D(a_i) = 1 \quad \text{and} \quad D'(a_i) = (a_i)^{-1} = \exp(+7)\,. \tag{38}$$

The $\gamma = 0$ integration is carried out from $a = a_i$ to an intermediate value of $a = a_\star$ (a free parameter corresponding to $z_\star = 1/a_\star - 1$), where the 2γ term, the other free parameter, is activated smoothly and persists up to the present epoch ($a = 1$, $z = 0$). The numerical algorithm uses the adaptive-step Runge-Kutta solver `ode45`, which has been widely employed in computational physics [36,37]. This solver automatically adjusts the step size to maintain accuracy, making it suitable for integrating the rapidly varying growth function over many orders of magnitude in scale factor a.

The resulting growth factors at $a = 1$ are then used to compute the corresponding linear clustering amplitude $S_8(\gamma)$ via

$$S_8(\gamma) = S_8(0)\left[\frac{D(a=1;\gamma)}{D(a=1;0)}\right] = S_8(0)\,\mathcal{D}_1(\gamma)\,, \tag{39}$$

where $S_8(0) = 0.8310$ is obtained from Equation (24) for $\gamma = 0$ and $\sigma_8(0) = 0.811$ [1], thereby allowing for a direct comparison with observational results.

The numerical solutions are controlled by the two free parameters γ and $z_\star$ (or $a_\star$) and are grouped into two sets (A and B) according to the chosen typical values of the parameter γ.

3.4.1. Parameter $\gamma \simeq 8\%$ of the Hubble Friction $2H(a)$

In the first set of solutions listed in Table 1, we choose $\gamma = 0.083$ and we determine the critical values of $z_\star$ and $a_\star$ that result in reduced growth at the present time relative to the standard ΛCDM

 doi:10.20944/preprints202601.1031.v1

solution. The reduced growth results in the listed values of $S_8 \in [0.75, 0.79]$, where one-half of the values determined by observations lie [15] (a total of $N = 38$ published measurements of $S_8 \in [0.7, 0.8]$, excluding 4 outliers, with mean $\bar{x} = 0.756$ and standard deviation $s = 0.026$). The complete solution with $\gamma = 0.083$ and $z \leq z_\star = 4.62$ that results in $S_8 = 0.77$ (Model A5 in Table 1) is illustrated in Figure 1.

Table 1. Numerical solutions of the growth Equation (31) with $\gamma = 0.083$ (i.e., 8.3% of the Hubble friction $2H$) at all redshifts $z \leq z_\star$.

γ	Model	$z_\star$	$a_\star$	$\mathcal{D}_1$	Growth Suppression $(1 - \mathcal{D}_1)$ (%)	S_8
0.083	A1	7.55	0.1170	0.9025	9.75	0.75
	A2	7.00	0.1250	0.9063	9.37	0.753
	A3	6.536	0.1327	0.9097	9.03	0.756
	A4	5.93	0.1443	0.9145	8.55	0.76
	A5	4.62	0.1779	0.9266	7.34	0.77
	A6	3.56	0.2193	0.9386	6.14	0.78
	A7	2.69	0.2710	0.9506	4.94	0.79

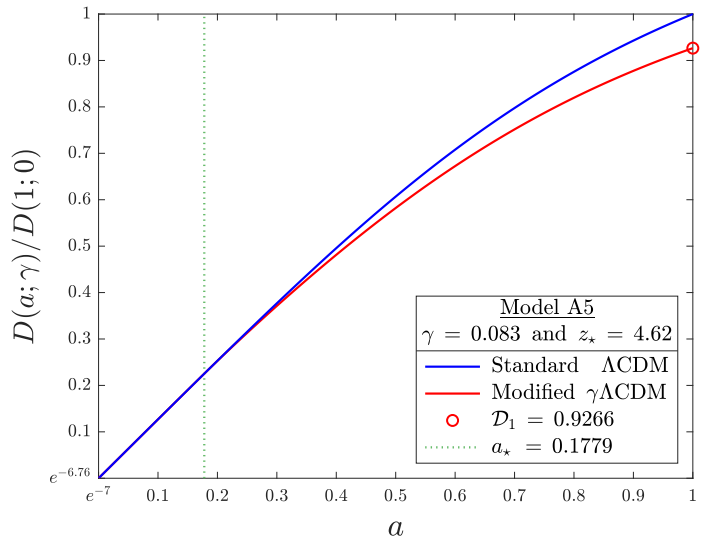

Figure 1. The numerical solution with $\gamma = 0.083$ and $z \leq z_\star = 4.62$ (red color) that results in $S_8 = 0.77$ (Model A5 in Table 1). The $\gamma = 0$ standard ΛCDM solution is also shown for comparison (blue color). Both solutions are normalized to the $a = 1$ value of the standard ΛCDM solution.

3.4.2. Parameter $\gamma \simeq 4\%$ of the Hubble Friction $2H(a)$

In the second set of solutions listed in Table 2, we choose $\gamma = 0.039$ and we analyze critical values of $z_\star < 10$ (perhaps a palatable upper limit [28]) that result in reduced growth at the present time. This smaller value of γ characterizes the smaller H_0 tension between standard ΛCDM [1] and a subset of the SnIa-TRGB measurements that have resulted in $H_0 \lesssim 70$ km s^{-1} Mpc^{-1} [15,17]. Evidently, drag forces of such a lower magnitude (only ~ 4% of the Hubble friction $2H$) are capable of resolving the S_8 tension only if S_8 truly lies at the high end (~0.79) of the observational range, and even then, $z_\star$ has to be ≥ 7, a relatively high threshold. The complete solution with $\gamma = 0.039$ and $z_\star = 7$ that results in $S_8 = 0.793$ (Model B3 in Table 2) is illustrated in Figure 2.

Table 2. Numerical solutions of the growth Equation (31) with $\gamma = 0.039$ (i.e., 3.9% of the Hubble friction $2H$) at all redshifts $z \leq z_\star$.

γ	Model	$z_\star$	$a_\star$	$\mathcal{D}_1$	Growth Suppression $(1 - \mathcal{D}_1)$ (%)	S_8
0.039	B1	9	0.1000	0.9475	5.25	0.787
	B2	8	0.1111	0.9506	4.94	0.790
	B3	7	0.1250	0.9540	4.60	0.793
	B4	6	0.1429	0.9578	4.22	0.796

Preprints.org (www.preprints.org) | NOT PEER-REVIEWED | Posted: 14 January 2026 doi:10.20944/preprints202601.1031.v1

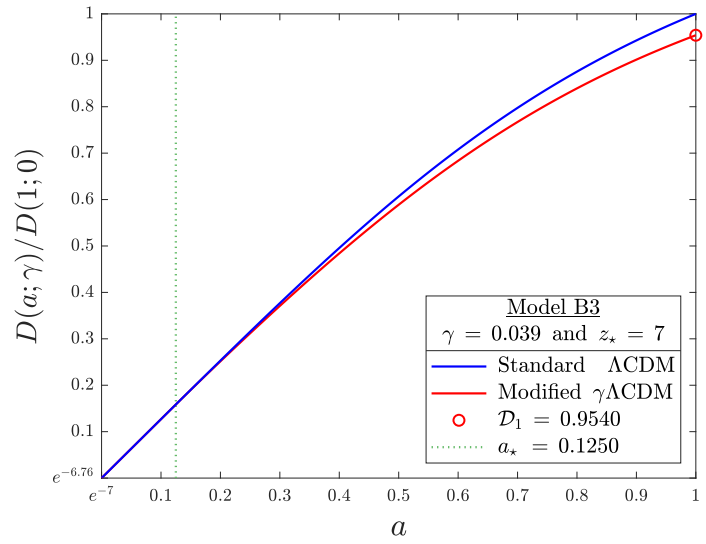

Figure 2. The numerical solution with $\gamma = 0.039$ and $z \leq z_\star = 7$ (red color) that results in $S_8 = 0.793$ (Model B3 in Table 2). The $\gamma = 0$ standard ΛCDM solution is also shown for comparison (blue color). Both solutions are normalized to the $a = 1$ value of the standard ΛCDM solution.

3.5. Growth Rate $f(a)$ from the Nonlinear First-Order Growth ODE

Another characterization of the linear growth of structure is provided by the dimensionless growth rate

$$f(a) \equiv \frac{d\ln D}{d\ln a}, \tag{40}$$

where the initial value problem (IVP) for $D(a)$ is described by Equations (31), (32), and (38) [26,28].

Recast in terms of $f(a)$, the IVP is described by a nonlinear first-order ODE of Riccati type, viz.

$$\frac{df(a)}{d\ln a} + \big(f(a)\big)^2 + \left(2(1+\gamma) - \frac{3}{2}\,\Omega_{\rm m}(a)\right) f(a) = \frac{3}{2}\,\Omega_{\rm m}(a)\,, \tag{41}$$

along with the initial condition

$$f(a_{\rm i}) = 1\,, \tag{42}$$

where $a_i = \exp(-7)$. Table 3 summarizes the present-day growth rates $f(1;\gamma)$ obtained for ΛCDM and the γΛCDM Models A1–A7 of Table 1. In general terms, the growth rates of the $\gamma > 0$ models are reduced by $\simeq 8\%$, in contrast to the $\mathcal{D}_1$ ratios that are reduced by 5–10%.

Table 3. Present-day growth rates $f(1;\gamma)$ obtained from numerical integrations of the IVP (41)-(42) for the models listed in Table 1. The first row shows the standard ΛCDM model. The last column shows the normalized ratio $\mathcal{F}_1 = f(1;\gamma)/f(1;0)$.

γ	Model	$z_\star$	$a_\star$	$\mathcal{D}_1$	$f(1;\gamma)$	$\mathcal{F}_1$
0	ΛCDM	···	···	1	0.52710	1
0.083	A1	7.55	0.1170	0.9025	0.48385	0.91795
	A2	7.00	0.1250	0.9063	0.48390	0.91803
	A3	6.536	0.1327	0.9097	0.48394	0.91812
	A4	5.93	0.1443	0.9145	0.48402	0.91826
	A5	4.62	0.1779	0.9266	0.48430	0.91880
	A6	3.56	0.2193	0.9386	0.48478	0.91971
	A7	2.69	0.2710	0.9506	0.48561	0.92128

The two diagnostics in Table 3, $\mathcal{D}_1$ copied from Table 1 and the new ratio $\mathcal{F}_1$, quantify different aspects of the same growth history:

 doi:10.20944/preprints202601.1031.v1

- Ratio $\mathcal{D}_1$ measures an integrated amplitude effect: once γ is activated at $a = a_\star$, the enhanced friction suppresses growth over the entire interval $a \in [a_\star, 1]$, and the accumulated suppression increases substantially when the activation redshift $z_\star$ is set farther into the past.
- By contrast, ratio $\mathcal{F}_1$ probes only a local logarithmic slope at the present epoch. Because this slope is determined mainly by the late-time background evolution (near $\Omega_{\rm m0}$) and the local friction term, varying $z_\star$ leaves the late-time slope $f(1;\gamma)$ largely unaffected. Consequently, the spread in $\mathcal{F}_1$ is much smaller than that in $\mathcal{D}_1$ across the $\gamma = 0.083$ models in Table 3.

3.5.1. Application: Models of Growth Rate $f(a) \propto (\Omega_{\rm m}(a))^n$

Table 4 summarizes two power-law representations of the numerically integrated linear growth rate $f(a)$ over the interval $a \in [a_\star, 1]$ for the models shown in Tables 1 and 3. The standard ΛCDM model [20] is also listed for comparison.

For each choice of $a_\star$, we solve the IVP (41)-(42) numerically across the interval $\mathcal{I}(a) = [a_{\rm i}, 1]$ and evaluate $f(a;\gamma)$ on a dense sampling in $(\ln a)$ space. Then, we perform two least-squares fits of the resulting curve in terms of the matter fraction $\Omega_{\rm m}(a)$: (a) a two-parameter $\{A, n\}$ fit of the standard form $f(a) = A\big(\Omega_{\rm m}(a)\big)^n$, and (b) a one-parameter $\{\ell\}$ fit of the form $f(a) = p_+\big(\Omega_{\rm m}(a)\big)^\ell$, in which the amplitude is fixed to the value $p_+ = 1 - 4\gamma/5$ predicted by the analytic model of Section 3.3 and only the exponent ℓ is optimized. Table 4 displays the best-fit parameters for each ansatz, along with a goodness-of-fit metric based on the RMS residuals over the interval $\mathcal{I}(a)$. A comparison between $\{A, n\}$ and $\{p_+, \ell\}$ isolates the deviation from a pure $(\Omega_{\rm m})^\ell$ power law that is absorbed by the floating normalization $A(a_\star)$ versus the pure power law in which the amplitude is constrained to be fixed ($p_+ = 0.9336$ for $\gamma = 0.083$).

Table 4. Power-law fits of growth rate $f(a)$ in $a \in [a_\star, 1]$: (a) two-parameter $\{A, n\}$ fit $f(a) = A\big(\Omega_{\rm m}(a)\big)^n$; and (b) one-parameter $\{\ell\}$ fit $f(a) = p_+\big(\Omega_{\rm m}(a)\big)^\ell$, where $p_+ = 1 - 4\gamma/5$ (Section 3.3) and $p_+ = 0.9336$ for $\gamma = 0.083$.

γ	Model	$z_\star$	$a_\star$	A	n	RMS Residual Error (%)	ℓ	RMS Residual Error (%)
0	ΛCDM	···	···	1.00011	0.55173	0.0423	0.55156	0.0436
0.083	A1	7.55	0.1170	0.95450	0.59635	1.31	0.56122	2.14
	A2	7.00	0.1250	0.95531	0.59727	1.30	0.56082	2.18
	A3	6.536	0.1327	0.95610	0.59814	1.29	0.56041	2.21
	A4	5.93	0.1443	0.95730	0.59940	1.27	0.55974	2.25
	A5	4.62	0.1779	0.96089	0.60281	1.21	0.55746	2.38
	A6	3.56	0.2193	0.96555	0.60656	1.12	0.55404	2.53
	A7	2.69	0.2710	0.97181	0.61065	1.00	0.54899	2.70

In Models A1–A7, the best-fit exponents are systematically higher than those determined for the ΛCDM model and listed in row 1 of Table 4 with $\gamma = 0$ and fitted parameters

$$\{A\,,\,n\} \;\simeq\; \{1\,,\,0.552\} \;\simeq\; \{p_+\,,\,\ell\}\,.$$

This is the expected model behavior in γΛCDM: for fixed $\Omega_{\rm m}(a)$, a higher power makes $f(a;\gamma)$ smaller at late times (when $\Omega_{\rm m} < 1$), reflecting the modest additional suppression of growth relative to standard ΛCDM. In this sense, the growth rates listed in Table 4 are consistent with the suppressed clustering amplitudes reported in Section 3.4.1 above.

 doi:10.20944/preprints202601.1031.v1

4. Modified Background Dynamics in $\gamma\Lambda$CDM

The drag force per unit mass introduced to the perturbed Euler Equation (12) in Section 2 has the effect of enhancing slightly the Hubble flow by a factor of $(1+\gamma)$, where $\gamma \ll 1$. Accounting for this enhancement in the kinematics of the flow, Equation (8) takes the form

$$\mathbf{u}(t,\mathbf{x}) \;=\; (1+\gamma)H(t)\mathbf{r} \;+\; \mathbf{v}(t,\mathbf{x})\,, \tag{43}$$

and the modified Hubble rate then affects the dynamics of the background Hubble expansion to $O(\gamma)$ in the $\gamma\Lambda$CDM model. The effect can be implemented in the dynamical Equations (3), (4), and (6) of Section 2.1 by substituting $H \to (1+\gamma)H$ and expanding terms to linear order in γ.

Below we analyze various diagnostics of the $\gamma\Lambda$CDM expansion, all related to the evolution of the Hubble rate $\dot{H}(t)$, which is discussed first.

4.1. Hubble-Rate Evolution

In the $O(\gamma)$ regime of $\gamma\Lambda$CDM, Equation (6) with $H \to (1+\gamma)H$ reads

$$2\dot{H} \;=\; \left(\Lambda c^2 \,-\, 3H^2\right) \,-\, \gamma\left(\Lambda c^2 \,+\, 3H^2\right), \tag{44}$$

or, in compact form,

$$2\dot{H} \;=\; -\,3H^2\left[(1-\Omega_\Lambda) \,+\, \gamma\,(1+\Omega_\Lambda)\right], \tag{45}$$

where

$$\Omega_\Lambda(t) \;\equiv\; \frac{\Lambda c^2}{3H^2}\,. \tag{46}$$

In the matter-dominated regime, where $\Omega_\Lambda(t) \ll 1$, we see that $\dot{H} = -3(1+\gamma)H^2/2 < 0$, and the $\gamma > 0$ factor always makes $\dot{H}$ more negative relative to its ΛCDM value. In fact, at any fixed H, the decrease of $H(t)$ is slightly faster in $\gamma\Lambda$CDM, and the location of the late-time attractor fixed point $H_{\rm fp}$ also changes slightly, as compared to the de Sitter value of $H_{\rm dS} = c\sqrt{\Lambda/3}$ (see below).

4.2. Hubble-Rate Fixed Point

Setting $\dot{H} = 0$ in the above equations for $2\dot{H}$, we derive the location of the fixed point of the late-time attractor to $O(\gamma)$, viz.

$$H_{\rm fp} \;=\; c\sqrt{\frac{\Lambda}{3}}(1-\gamma) \;=\; H_{\rm dS}(1-\gamma)\,, \tag{47}$$

or, equivalently,

$$(\Omega_\Lambda)_{\rm fp} \;=\; \frac{1+\gamma}{1-\gamma} \;\simeq\; 1 \,+\, 2\gamma \,+\, O(\gamma^2)\,. \tag{48}$$

The value of $(\Omega_\Lambda)_{\rm fp} > 1$ does not signal an inconsistency; rather, it reflects the fact that the standard closure relation $\Omega_m + \Omega_\Lambda = 1$ is modified in $\gamma\Lambda$CDM when the standard definitions of the ΛCDM parameters are retained (see Section 4.3): Equation (47) shows that $H_{\rm fp} < H_{\rm dS}$ since $\gamma > 0$, and Equation (48) follows directly from the standard definition of the parameter $\Omega_\Lambda \propto H^{-2}$ (Equation (46)). The end result is that the fixed point of the late-time attractor moves higher by $+2\gamma$ (see also Section 4.4).

At the expanding FLRW background level, the stability of the fixed point is not changed by γ to linear order. Considering Equation (44) in the form $\dot{H} = F(H)$, viz. $\dot{H}$ as a function of H, we find that

$$\frac{dF}{dH}(H = H_{\rm fp}) \;=\; -\,3H_{\rm dS} \,+\, O\left(\gamma^2\right) \;<\; 0\,.$$

Therefore, small perturbations $\delta H(t)$ about $H_{\rm fp}$ decay exponentially in time as $\delta H \propto \exp(-3H_{\rm dS}t)$.

 doi:10.20944/preprints202601.1031.v1

4.3. Vacuum and Matter Scaling

To interpret the γ modifications to the background dynamics, we recast the FEs in a form that makes the effective changes in the vacuum and matter couplings explicit. In the $O(\gamma)$ regime of $\gamma\Lambda$CDM, the first Friedmann Equation (4) reads

$$H^2 \;=\; (1-2\gamma)\left(\frac{\Lambda c^2}{3} \;+\; \frac{8\pi G\rho}{3}\right) \;+\; O(\gamma^2)\,. \tag{49}$$

Thus, the contributions of the dark and matter fields to H^2 are lowered by the same factor, and this is where our interpretation of an exterior tidal field comes in: a radially outward tidal force effectively counteracts the source of gravity ($\propto G\rho$) and also holds back the acceleration of the background. In effect, because of the $(1-2\gamma)$ scaling of Λ and ρ, the dark energy is pushing forward a little less, and gravity is pulling inward a little less (for more details, see Section 4.8 below).

We quantify the contribution of the outward field in the following manner: After some straightforward manipulations, we recast Equation (49) to the convenient $O(\gamma)$ form

$$\Omega_{\rm m}(t) \;+\; \Omega_\Lambda(t) \;=\; (1+\gamma)^2 \;=\; 1 \;+\; 2\gamma \;+\; O(\gamma^2)\,, \tag{50}$$

where $\Omega_{\rm m}(t) \equiv 8\pi G\rho/(3H^2)$ and $\Omega_\Lambda(t)$ is defined in Equation (46). Naturally, at the asymptotic limit $\Omega_{\rm m} \to 0$, Equation (50) reduces to Equation (48) of the fixed point of the late-time attractor.

4.4. Cosmic Acceleration

In this part, we consider the onset of the accelerated expansion in $\gamma\Lambda$CDM. We begin with the kinematic identity $\ddot{a}/a = \dot{H} + H^2$, which cannot be rescaled by hand, just as the kinematic definition of H (Equation (2)) cannot be rescaled. To build this identity in the $O(\gamma)$ regime, we rearrange the various terms in Equation (45), which becomes

$$2\left(\dot{H} \;+\; H^2\right) \;=\; H^2\left[(3\Omega_\Lambda \;-\; 1) \;-\; 3(1+\Omega_\Lambda)\,\gamma\right] \;=\; 2\frac{\ddot{a}}{a}\,. \tag{51}$$

Then, the condition $\ddot{a} \geq 0$ is satisfied at all times for which

$$\Omega_\Lambda(t) \;\geq\; \frac{1+3\gamma}{3(1-\gamma)} \;=\; \frac{1+4\gamma}{3} \;+\; O(\gamma^2)\,. \tag{52}$$

We proceed to determine the onset of acceleration in redshift space: For convenience, we calculate the derivative

$$\frac{d\Omega_\Lambda}{d(\ln a)} \;=\; \frac{\dot{\Omega}_\Lambda}{H} \;=\; -\,2\Omega_\Lambda\frac{\dot{H}}{H^2}\,; \tag{53}$$

using Equation (45) and the definition of redshift $z \equiv 1/a - 1$, we find a logistic-type Riccati ODE, viz.

$$\frac{d\Omega_\Lambda}{d(\ln a)} \;=\; -\,(1+z)\frac{d\Omega_\Lambda}{dz} \;=\; 3\Omega_\Lambda\Big[(1+\gamma) \;-\; (1-\gamma)\Omega_\Lambda\Big]\,. \tag{54}$$

In what follows, we do not display the closed-form solution $\Omega_\Lambda(z)$ of this first-order ODE, as it is cumbersome and adds little to our physical intuition. Instead, we integrate the ODE for various initial conditions $(\Omega_\Lambda)_{\rm rec}$ set at recombination ($\ln a_{\rm i} = -7$, $z_{\rm rec} = 1096$) to construct the phase portraits shown in Figure 3 for $\gamma = 0$ (ΛCDM) and $\gamma = 0.083$ ($\gamma\Lambda$CDM). In each portrait, the particular solution that matches the present-day condition $\Omega_{\Lambda 0} = 0.685$ [1] is singled out by a thick red curve, and the fixed point $(\Omega_\Lambda)_{\rm fp}$ is indicated by a horizontal dashed line.

 doi:10.20944/preprints202601.1031.v1

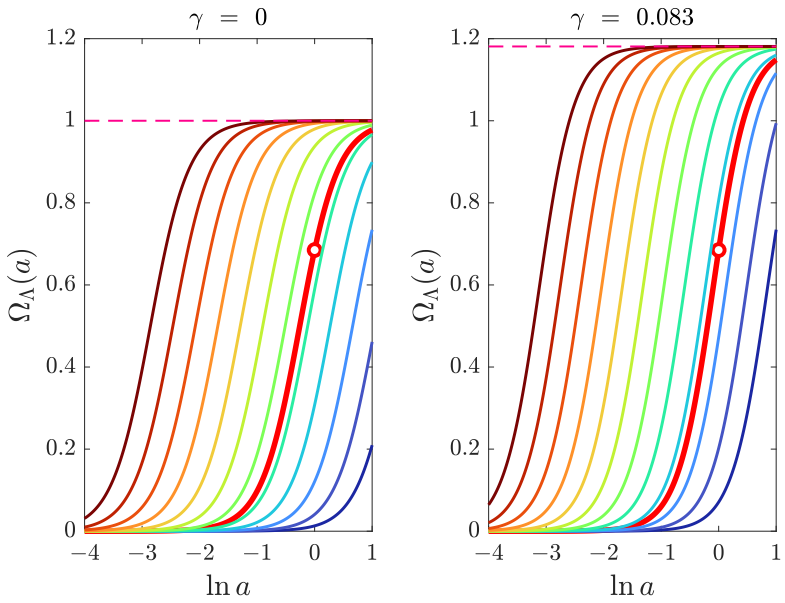

Figure 3. Phase portraits of the Riccati ODE (54) for $\gamma = 0$ (ΛCDM) and $\gamma = 0.083$ ($\gamma\Lambda$CDM). In each panel, the thick red curve denotes the particular solution that passes through $\Omega_{\Lambda 0} = 0.685$ (red circle), and the horizontal dashed line indicates the location of the late-time attractor fixed point (Equation (48)).

Next, we formulate the evolution of $\Omega_\Lambda(z)$ as a Cauchy problem implied by the definition (46) together with the $O(\gamma)$ modified Hubble dynamics, and we integrate Equation (54) subject to the present-day condition

$$\Omega_\Lambda(z = 0) \;=\; \Omega_{\Lambda 0}\,. \tag{55}$$

The resulting solutions are strictly monotonic: for any choice of $\gamma > 0$, parameter $\Omega_\Lambda(z)$ rises from negligible values at high redshifts to $\Omega_{\Lambda 0}$ at present, and tends to the attractor (48) at much later times. In this way, γ generates a one-parameter family of past and future histories, $\Omega_\Lambda(z;\gamma)$, including the standard ΛCDM evolution with $\gamma = 0$. Figure 4 illustrates the future trajectories of three family members with $\gamma \in [0,\, 0.039,\, 0.083]$.

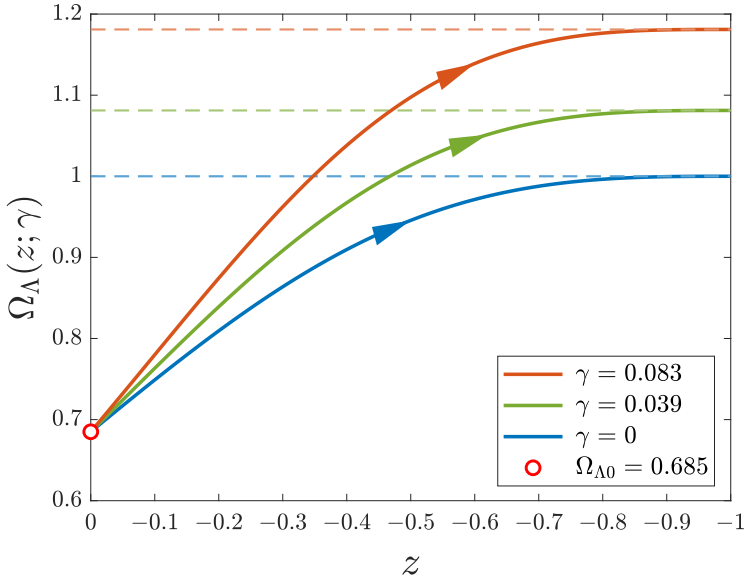

Figure 4. Future trajectories of the Cauchy problem (54)-(55) with $\gamma \in [0,\, 0.039,\, 0.083]$ are plotted versus redshift $z \le 0$. The red circle represents the initial condition $\Omega_{\Lambda 0} = 0.685$. The dashed lines indicate the corresponding locations of the late-time attractor fixed points (Equation (48)).

 doi:10.20944/preprints202601.1031.v1

4.4.1. Application: The $\ddot{a} = 0$ Transition Redshift

In the solutions of the Cauchy problem (54)-(55), the inequality $\ddot{a} \geq 0$ is satisfied for redshifts $z \leq z_T(\gamma)$. To continue our assessment, we choose $\gamma = 0.083$ and we solve the Cauchy problem to determine $z_T(\gamma = 8.3\%)$. Using the Planck-2018 condition that $\Omega_{\Lambda 0} = 0.685$ [1], we find that

$$z_T(\gamma = 8.3\%) \;=\; 0.2767\,, \tag{56}$$

a threshold to be compared to the ΛCDM value of $z_T(\gamma = 0) = (2\Omega_{\Lambda 0}/\Omega_{m0})^{1/3} - 1 = 0.6323$.

The dramatic decrease of z_T in $\gamma\Lambda$CDM is a nonlinear $[\Omega_\Lambda(z)]^2$ effect that can be traced to the Riccati ODE (54), although the γ modification also pushes z_T lower by raising the threshold value of $\Omega_\Lambda(z_T)$. The γ-modified nonlinear Riccati term displaces the late-time attractor (Equation (48)) to a higher value, and the higher fixed point selects a different family of trajectories, as compared to the ΛCDM fixed point of $(\Omega_{\Lambda CDM})_{fp} = 1$. Together, these two effects manage to reduce $z_T(\gamma = 8.3\%)$ relative to $z_T(\gamma = 0)$ by more than 50%.

4.5. Matter–Vacuum Equality Threshold

We now turn to the "matter–vacuum equality" (MVE) threshold underlying the DCP in standard ΛCDM (Section 1.1). This "recent" threshold, $z_{eq}(\gamma)$, is also modified in $\gamma\Lambda$CDM relative to the standard ΛCDM value of $z_{eq}(\gamma = 0) = (\Omega_{\Lambda 0}/\Omega_{m0})^{1/3} - 1 = 0.2956$.

For $\gamma > 0$, the same tidal field that modifies the background dynamics also modifies the effective dilution of matter. In fact, this dual action is the key reason that makes $\gamma\Lambda$CDM a successful model, and it will be discussed in more detail in Sections 4.8 and 5. In the matter sector of $\gamma\Lambda$CDM, the solution $\rho(z)$ of the $(1+\gamma)$-modified continuity Equation (3) is

$$\rho(z) \;=\; \rho_0(1+z)^{3(1+\gamma)}\,, \qquad \rho_0 \equiv \rho(z=0)\,, \tag{57}$$

so that the threshold of matter–vacuum equality $\rho(z_{eq}) = \rho_\Lambda$ (where $\rho_\Lambda \equiv \Lambda c^2/(8\pi G) = \text{const.}$) is reached at a different redshift $z_{eq}(\gamma)$ than in the $\gamma = 0$ ΛCDM.

Equating $\rho(z_{eq})$ to the constant vacuum density ρ_Λ, replacing the densities by their Ω parameters, and solving for $z_{eq}(\gamma)$, we find that

$$z_{eq}(\gamma) \;=\; \left(\frac{\Omega_{\Lambda 0}}{\Omega_{m0}}\right)^{\frac{1}{3(1+\gamma)}} \;-\; 1\,. \tag{58}$$

Using Planck-2018 values [1] and $\gamma = 0.083$, we obtain

$$z_{eq}(\gamma = 8.3\%) \;=\; 0.2701\,, \tag{59}$$

a value that is lower than $z_{eq}(\gamma = 0) = 0.2956$ by 8.6%.

4.5.1. Application: No Density Coincidence Problem in $\gamma\Lambda$CDM

At this point, we can compare the $\gamma = 0.083$ redshift thresholds of Equations (56) and (59). We find that

$$\frac{z_T - z_{eq}}{z_{eq}} \;\simeq\; 2.4\%\,, \tag{60}$$

that is, the acceleration threshold was crossed only 65 Myr before the MVE threshold was reached. Furthermore, each of these redshift thresholds differs from the mean $\bar{z} = 0.2734$ by only ±1.2%, where $\bar{z}$ corresponds to a lookback time of 3.28 Gyr in the standard ΛCDM universe of age 13.8 Gyr [1].

Preprints.org (www.preprints.org) | NOT PEER-REVIEWED | Posted: 14 January 2026 doi:10.20944/preprints202601.1031.v1

Based on these numerical results, we can argue that the DCP is effectively absent in $\gamma\Lambda$CDM: the $O(\gamma)$ onset of the accelerated epoch nearly coincides with the MVE threshold, with corresponding densities (relative to the present-day density ρ_0) of

$$\rho(z_{\rm T} = 0.2767) \;=\; 2.211\rho_0\,, \tag{61}$$

and

$$\rho(z_{\rm eq} = 0.2701) \;=\; 2.175\rho_0\,, \tag{62}$$

respectively, showing a relative difference of merely 1.7%. Figure 5 summarizes the matter density profiles and the corresponding thresholds for both ΛCDM models ($\gamma = 0,\ 0.083$) in the recent epoch with $z \in [0,\, 0.7]$.

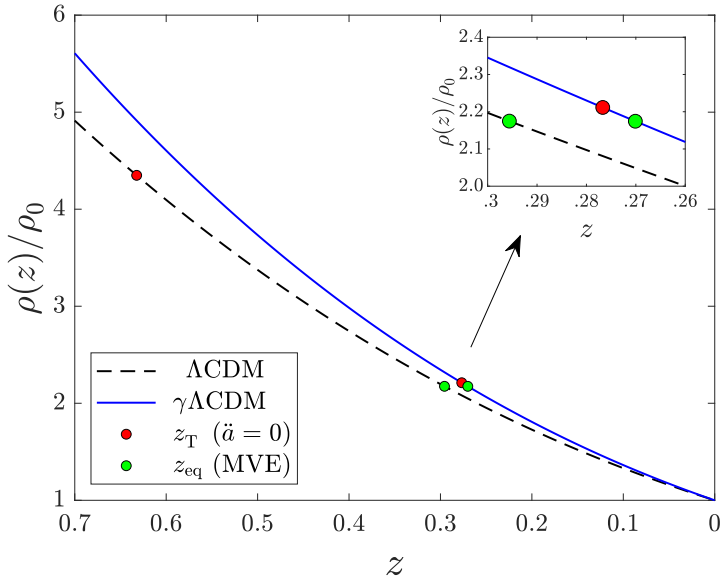

Figure 5. Matter density profiles in ΛCDM and $\gamma\Lambda$CDM ($\gamma = 0.083$) for $z \in [0, 0.7]$ plotted in reverse. The corresponding thresholds $z_{\rm T}$ and $z_{\rm eq}$ are marked by red and green dots, respectively.

4.6. Deceleration Parameter

The deceleration parameter is defined kinematically by

$$q \;\equiv\; -\frac{\ddot{a}/a}{H^2} \;=\; -1 \,-\, \frac{\dot{H}}{H^2}\,. \tag{63}$$

Using Equation (45), the $O(\gamma)$ deceleration parameter reads

$$q \;=\; \frac{1-3\Omega_\Lambda}{2} \,+\, \frac{3(1+\Omega_\Lambda)}{2}\,\gamma\,. \tag{64}$$

The γ term increases q in the matter-dominated epoch, and the deceleration $\ddot{a} = -qaH^2$ is stronger at fixed H. Thus, the transition point $\ddot{a}(z_{\rm T}) = 0$ occurs at a lower redshift $z_{\rm T}$ or, equivalently, at a higher value of $\Omega_\Lambda(t)$, as seen in Equation (52).

Equation (64) highlights some interesting properties of the deceleration parameter in $\gamma\Lambda$CDM: We adopt the ΛCDM form of $q(\gamma = 0) \equiv q^{(0)}$, viz.

$$q^{(0)} \;=\; \frac{1-3\Omega_\Lambda}{2}\,, \tag{65}$$

and we use it to eliminate Ω_Λ from Equation (64), which then takes the compact $O(\gamma)$ form

$$q \;=\; q^{(0)} \,+\, \gamma\big(2 \,-\, q^{(0)}\big)\,. \tag{66}$$

 doi:10.20944/preprints202601.1031.v1

Besides its simplicity, Equation (66) is also physically important for the following reasons:

- Since $q^{(0)} \leq 1$ in ΛCDM and $\gamma > 0$, the $O(\gamma)$ term increases q, and since $\ddot{a} \propto -q$, the difference

$$\Delta q \equiv q - q^{(0)} = \gamma(2 - q^{(0)}), \tag{67}$$

makes $\ddot{a}/a$ more negative at fixed H and enhances deceleration (or holds back acceleration in the corresponding regime), as noted above in the discussion of Equation (64).

- The $O(\gamma)$ difference Δq is modulated by ΛCDM baseline kinematics through the factor $(2 - q^{(0)})$. In particular, $\Delta q \to \frac{3}{2}\gamma$ (matter domination) and $\Delta q \to 3\gamma$ (Λ domination). Thus, the same constant γ produces an $O(1)$ larger correction in the acceleration era than in the deceleration era, with the magnitude of Δq remaining bounded across all intermediate epochs.
- The acceleration transition point $\ddot{a} = 0$ occurs when $q = 0$, and it is shifted in γΛCDM to

$$q^{(0)} = -\frac{2\gamma}{1-\gamma} = -2\gamma + O(\gamma^2). \tag{68}$$

This is a kinematic statement that the $\gamma > 0$ modification delays the onset of acceleration until redshift $z_T(\gamma)$ relative to the higher ΛCDM threshold of $z_T(\gamma = 0)$.

- The γΛCDM model does not permit an arbitrary z-dependent departure of the deceleration history $q(z)$. To $O(\gamma)$, the deviation Δq is proportional to the constant parameter γ (Equation (67)). Hence, varying γ only rescales a definite, model-prescribed departure of $q(z)$ (relative to $\gamma = 0$ ΛCDM), rather than introducing a free correction function of z. Consequently, observational reconstructions of $q(z)$—from distance indicators or via the transition redshift z_T—can constrain the parameter γ directly.

4.6.1. Application: Present-Day Deceleration Parameter

Applying Equation (64) with $\gamma = 0.083$ to the present time ($\Omega_{\Lambda 0} = 0.685$ [1]), we find that

$$q(z = 0) = -0.318. \tag{69}$$

Compared to the corresponding ΛCDM value of -0.528 [38], the magnitude of $q(z = 0)$ is reduced by about 40%. This implies that the present-day acceleration $\ddot{a}$ is nearly 40% smaller in γΛCDM.

4.7. Effective Equation of State

In the standard FLRW framework (cf. [38]), the deceleration diagnostic may be written as

$$q = \frac{1}{2}(1 + 3w_{\rm tot}), \tag{70}$$

where the total EOS index $w_{\rm tot} = P_{\rm tot}/(\rho_{\rm tot}c^2)$ is determined by the total pressure $P_{\rm tot} = P + P_\Lambda$ and density $\rho_{\rm tot} = \rho + \rho_\Lambda$. This relation remains valid in our treatment because in the Friedmann Equation (49) both contributions to H^2 are modified by the same constant factor $(1 - 2\gamma)$. Then, the matter pressure P appears to be nonzero, but it does not come from the dust; the solution (57) of the $(1 + \gamma)$-modified continuity equation shows that, effectively,

$$P(\rho; \gamma) = \gamma\rho c^2, \tag{71}$$

an EOS that corresponds to an effective index

$$w_\gamma = \gamma. \tag{72}$$

So, in γΛCDM, we have two contributions to $w_{\rm tot}$, the effective index w_γ and the index $w_\Lambda = -1$ of the cosmological dark fluid with negative pressure $P_\Lambda = -\rho_\Lambda c^2$.

 doi:10.20944/preprints202601.1031.v1

On the other hand, the modified Friedmann Equation (49) alters the standard sum rule $\Omega_{\rm tot} = 1$ to the $\gamma\Lambda$CDM rule

$$\Omega_{\rm tot} \equiv \Omega_{\rm m} + \Omega_\Lambda = 1 + 2\gamma + O(\gamma^2), \tag{73}$$

as is also seen in Equation (50). Then, the total index $w_{\rm tot}$ is determined from the weighted average

$$w_{\rm tot} = \frac{-\Omega_\Lambda + \gamma\,\Omega_{\rm m}}{\Omega_{\rm tot}}, \tag{74}$$

or, equivalently, from the $O(\gamma)$ equation

$$w_{\rm tot} = -\Omega_\Lambda + \gamma(1 + \Omega_\Lambda). \tag{75}$$

Substituting Equation (75) into (70) reproduces Equation (64), which indicates that the $O(\gamma)$ modifications of the FEs can be described within the relativistic FLRW framework by an effective pressure term, $P(\rho;\gamma) = \gamma\rho c^2$, assigned to the matter sector along with the modified sum rule (73).

4.7.1. Application: Present-Day Effective EOS Index

To make a connection with the standard two-component general relativistic phenomenology (presureless matter plus a single dark fluid), we introduce an effective dark-energy index $w_{\rm eff}$ defined as the constant EOS index which reproduces the same deceleration $q_0 \equiv q(z=0)$ in a universe of dust. According to this definition, the effective index reads [38]

$$w_{\rm eff}(z=0) = \frac{2q_0 - 1}{3\Omega_{\Lambda 0}}. \tag{76}$$

Using $\Omega_{\Lambda 0} = 0.685$ [1] and Equation (69), we obtain

$$w_{\rm eff}(z=0) = -0.796, \tag{77}$$

corresponding to a shift of $\Delta w_{\rm eff} \simeq +0.20$ relative to the ΛCDM value of $w_\Lambda = -1$. Here, $w_{\rm eff}$ is introduced as a purely phenomenological mapping to the usual "dust plus dark-energy" fit and should not be confused with the EOS indices w_γ and $w_{\rm tot}$ evaluated above.

4.8. Global Energy Conservation

The $O(\gamma)$ modifications discussed in Section 4.3 can be thought as arising from an isotropic tidal field described by a stress–energy tensor $T^{(\rm tid)}_{\mu\nu}$ in the Einstein field equations, viz.

$$G_{\mu\nu} = \frac{8\pi G}{c^4}\left(T^{(\rm mat)}_{\mu\nu} + T^{(\rm vac)}_{\mu\nu} + T^{(\rm tid)}_{\mu\nu}\right), \tag{78}$$

where superscripts also label the matter sector and the vacuum sector. Each component is taken to be a perfect fluid comoving with the background four-velocity u^μ. The matter and vacuum sectors obey the usual ΛCDM properties, viz. $\{\rho > 0,\ P = 0\}$ for dust and

$$\{\rho_\Lambda = \text{const.} > 0,\quad P_\Lambda = -\rho_\Lambda c^2 < 0\}, \tag{79}$$

for vacuum, respectively.

In this framework, the vacuum–matter coupling Equation (49) takes the form

$$\rho_{\rm c} = (1 - 2\gamma)(\rho + \rho_\Lambda) + O(\gamma^2), \tag{80}$$

where the critical FLRW density $\rho_{\rm c}(a)$ is given by Equation (26). This equation implies that the $O(\gamma)$ effective tidal density is

$$\rho_{\rm tid} = -2\gamma(\rho + \rho_\Lambda). \tag{81}$$

 doi:10.20944/preprints202601.1031.v1

Thus, at the background level, the tidal sector provides a screening contribution that produces the particular $(1-2\gamma)$ rescaling of both the matter and vacuum sectors in Equations (49) and (80).

The continuity equation is derived from the contracted Bianchi identity of the Einstein tensor, viz. $\nabla^{\mu}G_{\mu\nu}=0$, which enforces conservation of the total stress–energy tensor in Equation (78). In the flat FLRW background, the vacuum terms do not appear in the continuity equation and global energy conservation is expressed by a pair of coupled equations, viz.

$$\dot{\rho} + 3H\rho = +Q\,, \tag{82}$$

$$\dot{\rho}_{\rm tid} + 3H\left(\rho_{\rm tid} + P_{\rm tid}/c^2\right) = -Q\,, \tag{83}$$

where the $\gamma\Lambda$CDM rate

$$Q(t) = -3\gamma H\rho\,, \tag{84}$$

encodes the energy transfer between dust and the effective tidal reservoir (whereas ρ_{Λ} and P_{Λ} remain strictly constant in time).

Equation (82) is the $(1+\gamma)$-modified FLRW continuity equation for dust (as compared to the ΛCDM Equation (3)). Equation (83) helps determine the effective tidal pressure $P_{\rm tid}$ as follows: differentiating Equation (81) with respect to cosmic time and setting $\dot{\rho}_{\Lambda}=0$, we find that $\dot{\rho}_{\rm tid}=-2\gamma\dot{\rho}$ and, to $O(\gamma)$, that $\dot{\rho}_{\rm tid}=6\gamma H\rho$. Then, Equation (83), solved for $P_{\rm tid}$, is reduced to the form

$$P_{\rm tid} = \gamma\left(\rho + 2\rho_{\Lambda}\right)c^2 + O\left(\gamma^2\right). \tag{85}$$

Equations (81)–(85) demonstrate that the $\gamma\Lambda$CDM background evolution, as described by Equations (49) and (80), admits a fully conservative interpretation in which energy–momentum is redistributed between the dust sector and the isotropic tidal sector, while the global relativistic conservation law $\nabla^{\mu}G_{\mu\nu}=0$ is exactly preserved to linear order in the parameter γ. In particular, when the above relations are recast into the conventional two-component form (dust plus a single dark fluid), they reproduce to $O(\gamma)$ the effective EOS index $w_{\rm eff}(z=0)=-0.796$ of Section 4.7.1.

Equations (81) and (85) show that the tidal sector is characterized by a negative energy density $\rho_{\rm tid}<0$ and a positive pressure $P_{\rm tid}>0$, with both quantities evolving in time. The signs are opposite to those of the density and pressure of the vacuum sector (Equation (79)). More generally, any time-dependent dark component (or exotic field) with the same sign structure—entering the Einstein field Equations (78) in the same manner as the stress–energy tensor $T^{(\rm tid)}_{\mu\nu}(\rho_{\rm tid},P_{\rm tid})$—could provide an alternative source/origin of the modified kinematics and dynamics produced by $\gamma\Lambda$CDM. The essential requirement is that such a dark component or field $T_{\mu\nu}(\gamma)$ must simultaneously rescale the effective contributions of both the matter and vacuum sectors to the expansion history to $O(\gamma)$ as follows:

$$\begin{aligned} \rho_{\rm tot} &= +(1-2\gamma)(\rho+\rho_{\Lambda})\,,\\ P_{\rm tot} &= -(1-2\gamma)\rho_{\Lambda}c^2 + \gamma\rho c^2\,. \end{aligned} \tag{86}$$

In this fundamental set of $\gamma\Lambda$CDM equations, notice, in particular, the dual action of the reduction factor $(1-2\gamma)$ on to both ρ and ρ_{Λ} (cf. Equation (49)), as well as the remarkable appearance of the "dust pressure" term given by Equation (71)—which, of course, does not come from the dust, but it is traced to the $(1+\gamma)$-modified matter continuity Equation (82).

We do note however that the specific $T^{(\rm tid)}_{\mu\nu}$ modification of Equations (78) or other sources of $T_{\mu\nu}(\gamma)$ modifications supporting Equations (86) effectively rule out exotic dark fields that require effective EOS indices $w_{\rm eff}(z=0)<-1$ or total EOS indices $w_{\rm tot}<-1$ (see Section 4.7).

 doi:10.20944/preprints202601.1031.v1

4.8.1. Application: Tidal-Sector EOS Index

In $\gamma\Lambda$CDM, the tidal sector itself admits a well-defined, albeit time-dependent, EOS index, viz.

$$w_{\rm tid}(a) \equiv \frac{P_{\rm tid}}{\rho_{\rm tid}c^2} = -\frac{1}{2}\left(1 + \frac{\rho_\Lambda}{\rho(a) + \rho_\Lambda}\right) = -1 + \frac{1}{2}\,\Omega_{\rm m}(a)\,, \tag{87}$$

where $\Omega_{\rm m}(a)$ is given by Equation (32). At the present epoch, $\Omega_{\rm m0} = 0.315$ [1] and

$$w_{\rm tid}(a=1) = -0.8425\,. \tag{88}$$

In the Λ-dominated de Sitter future $a \to \infty$, then $\Omega_{\rm m} \to 0$ and $w_{\rm tid} \to -1$. In this asymptotic limit, the tidal density and pressure saturate to $\rho_{\rm tid} \to -2\gamma\rho_\Lambda < 0$ and $P_{\rm tid} \to +2\gamma\rho_\Lambda c^2 > 0$, respectively, where they continue to modify to $O(\gamma)$ the Hubble flow $H(t)$ (Equations (49) and (80)) and partially counteract the background acceleration $\ddot{a}(t)$. But note that the sign structure of the tidal field is markedly opposite to that of the constant Λ field. This generally means that any introduced exterior field replacing the tidal field $T^{(\rm tid)}_{\mu\nu}$ must also have negative energy density and positive pressure.

4.9. ΛCDM–$\gamma\Lambda$CDM Comparison

For comparison purposes, Table 5 lists several widely known parameter values of standard ΛCDM and the corresponding values obtained in this work from the benchmark $\gamma\Lambda$CDM model with $\gamma = 0.083$.

The most remarkable difference appears in row 6 which shows the transition redshift $z_{\rm T}$ of the inflection point $\dddot{a} = 0$. The benchmark $\gamma\Lambda$CDM value of $z_{\rm T}$ has shifted down to the level of the MVE redshift (row 8). The nonlinearity responsible for this large shift was discussed in Section 4.4.1. Besides the dramatic decrease of the $z_{\rm T}$ threshold, (a) the LSS parameter S_8 has clearly decreased to the serviceable range required by observations, resolving thus the S_8 tension (row 3); and (b) the effective Λ-EOS index $w_{\rm eff}(z=0)$ is now $\simeq -0.80$ in $\gamma\Lambda$CDM, rather than -1 in standard ΛCDM (row 11).

Table 5. Comparison of Results between Standard ΛCDM ($\gamma = 0$) and Benchmark $\gamma\Lambda$CDM ($\gamma = 0.083$).

Row #	Parameter	Symbol	ΛCDM Value ($\gamma = 0$)	$\gamma\Lambda$CDM Value ($\gamma = 0.083$)
1	Hubble Constant	H_0	—— 67.4 km s^{-1} Mpc^{-1} ——	
2	Dark-Energy Fraction	$\Omega_{\Lambda 0}$	——— 0.685 ———	
3	LSS Parameter	S_8	$\simeq 0.83$	$\simeq 0.77$
4	Hubble Friction	$2(1+\gamma)H(t)$	$2H(t)$	$2.166H(t)$
5	Fixed Point	$(\Omega_\Lambda)_{\rm fp}$	1	1.166
6	Transition Redshift	$z_{\rm T}$	0.6323	0.2767
7	Zero–Acceleration Ω_Λ	$\Omega_\Lambda(z_{\rm T})$	$\frac{1}{3}$	0.454
8	MVE Redshift	$z_{\rm eq}$	0.2956	0.2701
9	MVE Ω_Λ	$\Omega_\Lambda(z_{\rm eq})$	$\frac{1}{2}$	$\simeq 0.6$
10	Deceleration Parameter	$q(z=0)$	-0.528	-0.318
11	Effective Λ-EOS Index	$w_{\rm eff}(z=0)$	-1	-0.796
12	Total EOS Index	$w_{\rm tot}(z=0)$	-0.685	-0.545
13	Tidal-Sector EOS Index	$w_{\rm tid}(z=0)$	···	-0.8425
14	"Dust-EOS" Index	w_γ	···	0.083

 doi:10.20944/preprints202601.1031.v1

5. The Dual Action of the Tidal Field in $\gamma\Lambda$CDM

We noted in Section 4 that the dual action of the radial tidal field (Equation (49)) distinguishes $\gamma\Lambda$CDM from other models that modify gravity/drag or the background dark energy, but not both at the same time [13–15]. This dual action can also be seen in Table 5 by comparing the results listed in rows 3–4 and 11–12, respectively.

Here, we analyze a simplified model of tidal forces that can systematically bias CDL inferences of H_0 toward higher values relative to the ΛCDM–CMB outcome. The main idea is that along an observer's line of sight (LOS) leading to a low-redshift target at $r = r_0$, there are always more nearby nonlinear perturbers at distances $r > r_0$ than on the side of the observer at $r = 0$. This is independent of the observer's location lying at the origin $r = 0$.

5.1. Preliminaries

We assume a spherical isotropic distribution or perturbers that can be reduced to an effective 1-D radial model along the observer's LOS. But we want to preserve the shell geometry of the 3-D distribution, so we adopt a "coherence" cone with a fixed solid angle $\Delta\Omega \ll 4\pi$ anchored at $r = 0$ and extending out to the Hubble radius $r_H \gg r_0$. However, the integrations will not extend that far, they will be limited by the assumption that nonlinear perturbers are formed at late times and their mean tidal field becomes active only for scale factors $a \geq a_\star$ (Section 3.4).

The target galaxy is assumed to have a physical radius $s_0 \ll r_0$, so there are no perturbers in the interval $|r - r_0| < s_0$ at a given epoch $a(t)$. In comoving coordinates $x = r/a$, the mean density of the perturbers is assumed to be

$$\overline{\rho}(a) \;=\; m\,\overline{n}(a)\,, \tag{89}$$

where m is a typical perturber mass and $\overline{n}$ is the comoving mean number density. Then, the section of a shell of width dx at distance x within the coherence cone contains mass $dM = \overline{\rho}\,\Delta\Omega\,x^2 dx$, and the comoving density per unit length then is

$$\mu(x) \;=\; \frac{dM}{dx} \;=\; (\overline{\rho}\,\Delta\Omega)x^2\,, \tag{90}$$

excluding the interval $|x - x_0| < \sigma_0$, where $x_0 = r_0/a$ and $\sigma_0 = s_0/a \ll x_0$. Then, the radial profile (90) has the domain

$$x \;\in\; \left[\max(0,\, x_0 - x_\star)\,,\; x_0^-\right] \cup \left[x_0^+\,,\; x_0 + x_\star\right], \tag{91}$$

where $x_0^\pm = x_0 \pm \sigma_0 > 0$ and the cutoff scale $x_\star$ is determined from the requirement that $a \geq a_\star$ and the epoch of the observation $a = 1$ (Section 3.4). Specifically,

$$x_\star \;=\; c\int_{a_\star}^{1} \frac{da}{a^2 H(a)}\,, \tag{92}$$

and it specifies the conformal distance that a signal propagating at the speed of light c can traverse between $a = a_\star$ and $a = 1$ in a flat FLRW background.

5.2. Tidal Acceleration Components

First we derive the differential tidal acceleration along the observer's LOS produced by a perturbing mass element dM located at comoving radius x on to the target at x_0. The relevant Newtonian separation between the two galaxies is their physical separation

$$\Delta r \;=\; |r - r_0| \;=\; a\,\Delta x\,, \tag{93}$$

 doi:10.20944/preprints202601.1031.v1

where $\Delta x = |x - x_0|$ is the comoving separation. In the far-field regime (where $\Delta r \gg s_0$), the magnitude of the Newtonian tidal acceleration $d\mathrm{a}$ generated by an exterior mass dM then is

$$d\mathrm{a} \;=\; \frac{2Gs_0\,dM}{(\Delta r)^3} \;=\; \frac{2G\sigma_0\,dM}{a^2(\Delta x)^3}\,, \tag{94}$$

where $d\mathrm{a} > 0$ when it points away from the observer.

Using Equation (90), subtracting the interior from the exterior contribution, and integrating, we find that the net tidal acceleration of the target is

$$\mathrm{a}_{\rm net}(a) \;=\; \frac{2G\sigma_0}{a^2}\,(\overline{\rho}\,\Delta\Omega)\left\{\int_{x_0+\sigma_0}^{x_0+x_\star}\frac{x^2dx}{(x-x_0)^3} \;-\; \int_{\max(0,\,x_0-x_\star)}^{x_0-\sigma_0}\frac{x^2dx}{(x_0-x)^3}\right\}, \tag{95}$$

where $x_\star$ is given by Equation (92).

Using new variables $u = x - x_0$ for the exterior integral and $u = x_0 - x$ for the interior integral, we transform Equation (95) to the form

$$\mathrm{a}_{\rm net}(a) \;=\; \frac{2G\sigma_0}{a^2}\,(\overline{\rho}\,\Delta\Omega)\left\{\int_{\sigma_0}^{x_\star}\frac{(x_0+u)^2du}{u^3} \;-\; \int_{\sigma_0}^{\min(x_0,\,x_\star)}\frac{(x_0-u)^2du}{u^3}\right\}. \tag{96}$$

Performing the integrations in the regime of interest $x_0 < x_\star$, we find that

$$\mathrm{a}_{\rm net}(a) \;=\; \frac{8Gx_0}{a^2}\,(\overline{\rho}\,\Delta\Omega)\left\{1 \;-\; \frac{1}{8}\frac{\sigma_0}{x_0}\Big(3 + 2\ln\varepsilon + 4\varepsilon + \varepsilon^2\Big)\right\}, \tag{97}$$

where $\sigma_0/x_0 \ll 1$ and

$$\varepsilon \;\equiv\; \frac{x_0}{x_\star} \;<\; 1\,. \tag{98}$$

The zeroth-order term is clearly the most significant term in $\mathrm{a}_{\rm net}(a)$. Evaluating then the zeroth-order tidal acceleration for the present time, we set $a = 1$ and $x_0 = r_0$, and we determine that

$$\mathrm{a}^{(0)}_{\rm net}(a=1) \;=\; 32\pi G\,\overline{\rho}(a=1)\,r_0\Delta\omega \;+\; O\big(s_0/r_0\big)\,, \tag{99}$$

where $\overline{\rho}(a=1)$ is given by Equation (89) and $\Delta\omega = \Delta\Omega/(4\pi) \ll 1$ is the normalized solid angle of the coherence cone that we adopted for the 1-D radial model.

It is worth pointing out that $\mathrm{a}^{(0)}_{\rm net}$ is also obtained (much easier) by replacing the interior upper limit $\min(x_0,\, x_\star)$ by $x_\star$ in Equation (96). But then, the interior integration is extended past $x = 0$ and on to the opposite ray of the observer's LOS. In the 1-D radial model analyzed here, such a two-ray extension may be acceptable because some nonlinear perturbers "behind" the observer are within the same activation-limited causal range and contribute to the long-range tidal environment of the target galaxy.

5.3. Characteristic Estimates

We return to the comoving form of the zeroth-order tidal acceleration of Equation (97), viz.

$$\mathrm{a}^{(0)}_{\rm net}(a) \;=\; 32\pi G\,\frac{\overline{\rho}(a)}{a^2}\,x_0\,\Delta\omega\,, \tag{100}$$

and we approximate $\overline{\rho}(a)$ by $\overline{\rho}(1) = f_0\rho_0$, where f_0 is the present-day participation fraction of the perturber population, and

$$\rho_0 \;\equiv\; \frac{3\Omega_{\rm m0}H_0^{\,2}}{8\pi G}\,. \tag{101}$$

 doi:10.20944/preprints202601.1031.v1

The approximation is justified in practice as we are working in the $z < 10$ domain, when the perturber galaxies are already well-formed [39–41] and exert tidal forces throughout the domain of $a \in [a_\star, 1]$. Then, Equation (100) becomes

$$\mathrm{a}_{\mathrm{net}}^{(0)}(a) \;=\; 12\,\Omega_{\mathrm{m0}} H_0^{\,2}\,\frac{x_0}{a^2}\big(f_0\,\Delta\omega\big)\,, \tag{102}$$

and reduces at the present epoch to

$$\mathrm{a}_{\mathrm{net}}^{(0)}(a=1) \;=\; 12\,\Omega_{\mathrm{m0}} H_0^{\,2}\,r_0\big(f_0\,\Delta\omega\big)\,. \tag{103}$$

The parenthesis highlights the geometric factors that are sources of uncertainty in evaluations of the net tidal acceleration.

The recession speed due to the acceleration (102) accumulated up to the present is

$$\mathrm{v}_{\mathrm{rec}}(a=1) \;=\; \int_{a_\star}^{1} \frac{\mathrm{a}_{\mathrm{net}}^{(0)}(a)}{H(a)}\,\frac{da}{a}\,. \tag{104}$$

In the matter-dominated epoch of ΛCDM, the Hubble parameter is written as $H(a) = H_0 E(a)$, where the dimensionless function $E(a)$ is given by Equation (28). Then, Equation (104) takes the form

$$\mathrm{v}_{\mathrm{rec}}(a=1) \;=\; 12\,\Omega_{\mathrm{m0}} H_0\, r_0\big(f_0\,\Delta\omega\big)\,\mathcal{J}(a_\star)\,, \tag{105}$$

where the tidal activation integral $\mathcal{J}(a_\star)$ is given by

$$\mathcal{J}(a_\star) \;=\; \int_{a_\star}^{1} \frac{da}{a^3 E(a)}\,. \tag{106}$$

We can form now the dimensionless ratio $\mathrm{a}_{\mathrm{net}}^{(0)}/(H_0\,\mathrm{v}_{\mathrm{rec}})$ at $a = 1$ that, according to our heuristic drag model of Section 2, is a measure of the coefficient of friction 2γ. An added benefit is that the uncertain geometric factors and the distance to the target galaxy cancel out when Equation (103) is divided by Equation (105). Then, we find that

$$\gamma \;=\; \frac{1}{2\,\mathcal{J}(a_\star)}\,. \tag{107}$$

Thus, in this approximation, the zeroth-order 1-D radial model shows that γ is determined primarily by the tidal activation epoch $a_\star$ within the standard ΛCDM expanding background.

For $\Omega_{\Lambda 0} \neq 0$, the integral $\mathcal{J}(a_\star)$ does not admit a closed-form expression in terms of elementary functions, so in our estimates, we revert to numerical evaluations and a first-order approximation in the small parameter $(\Omega_{\Lambda 0}/\Omega_{\mathrm{m0}})a^3$. Expanding the integrand of $\mathcal{J}(a_\star)$ and the right-hand side of Equation (107) to first order, we find that

$$\gamma^{(1)} \;\simeq\; \frac{1}{4}\,\frac{\sqrt{\Omega_{\mathrm{m0}}\,a_\star}}{1-\sqrt{a_\star}}\left\{1 \;-\; \frac{1}{10}\left(\frac{\Omega_{\Lambda 0}}{\Omega_{\mathrm{m0}}}\right)\frac{\sqrt{a_\star}-a_\star^3}{\sqrt{a_\star}-1}\right\}. \tag{108}$$

Some representative results in which the resulting exact values of $\gamma \in [0.039, 0.083]$ are listed in Table 6 for the corresponding $a_\star$ and $z_\star = 1/a_\star - 1$ values, and for $\Omega_{\mathrm{m0}} = 0.315$ and $\Omega_{\blacksquare 0} = 0.685$ [1]. The zeroth-order approximation,

$$\gamma^{(0)} \;\simeq\; \frac{1}{4}\,\frac{\sqrt{\Omega_{\mathrm{m0}}\,a_\star}}{1-\sqrt{a_\star}}\,, \tag{109}$$

shows deviations from the exact numerical γ values by about 4–8%, and the first-order approximation (108) shows deviations of about 2–4%. The exact and approximate results are plotted in Figure 6.

 doi:10.20944/preprints202601.1031.v1

Table 6. Determined γ values in the 1-D radial model of this section. Exact values of γ were determined numerically from Equation (107) for the chosen $a_\star$ values. Approximate values $\gamma^{(0)}$ and $\gamma^{(1)}$ were determined from Equations (109) and (108), respectively, for the chosen $a_\star$ values. Percent deviations $\Delta\gamma^{(0)}$ and $\Delta\gamma^{(1)}$ from the exact values are also listed for comparisons. Finally, midpoint estimates of $\gamma^{(\mathrm{mid})}$ (Equation (110)) and their percent deviations are listed in the last two columns.

Model	$a_\star$	$z_\star$	S_8	γ	$\gamma^{(0)}$	$\Delta\gamma^{(0)}$ (%)	$\gamma^{(1)}$	$\Delta\gamma^{(1)}$ (%)	$\gamma^{(\mathrm{mid})}$	$\Delta\gamma^{(\mathrm{mid})}$ (%)
C1	0.045	21.22	0.768	0.0392	0.0378	−3.7	0.0400	+1.9	0.0389	−0.9
C2	0.075	12.33	0.760	0.0558	0.0529	−5.2	0.0573	+2.6	0.0551	−1.3
C3	0.100	9.00	0.756	0.0693	0.0649	−6.4	0.0714	+3.0	0.0681	−1.7
C4	0.125	7.00	0.753	0.0830	0.0767	−7.5	0.0858	+3.5	0.0813	−2.0

Notes. (a) The $z_\star$ values were calculated from $z_\star = 1/a_\star - 1$. (b) The S_8 values were computed by numerical integrations (see Section 3.4) for the listed pairs of $(a_\star, \gamma)$. (c) There is no S_8 tension in the 1-D radial model because the tidal field is activated too early in redshift space ($z_\star \geq 7$). (d) Model C4, a palatable model, is also listed in Table 1 as Model A2.

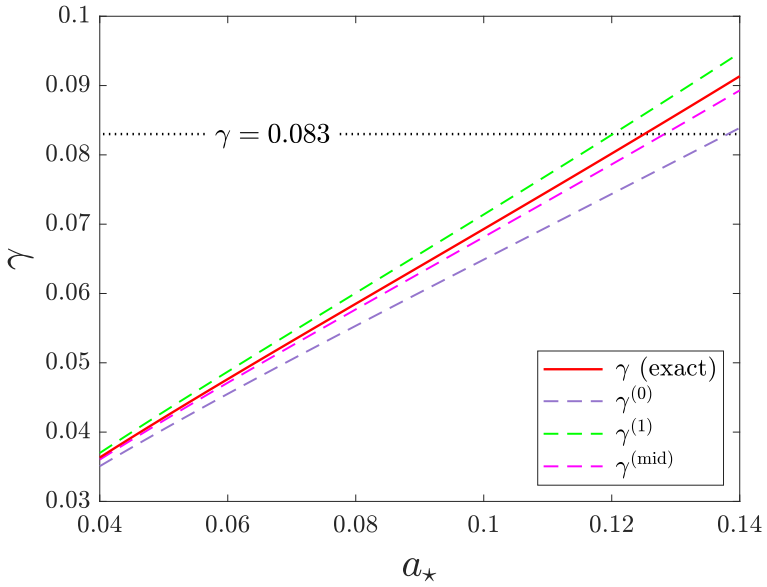

Figure 6. Exact and approximate values of γ versus $a_\star$ in the 1-D radial model of Section 5. The exact values were computed numerically from Equation (107), and the approximate values were calculated from Equations (108)–(110).

For the tidal activation scales of $a_\star \in [0.045, 0.125]$ in Table 6, the exact γ values are bracketed by the approximate analytic values, with $\gamma^{(0)}$ underpredicting and $\gamma^{(1)}$ overpredicting the exact results (Figure 6). For this reason, analytic values of higher accuracy can be obtained by the midpoint estimator

$$\gamma^{(\mathrm{mid})} \;=\; \frac{1}{2}\left(\gamma^{(0)} + \gamma^{(1)}\right), \tag{110}$$

without having to calculate the next higher-order approximation. This amounts to simply halving the coefficient $\frac{1}{10}$ of the correction term in Equation (108) and results in deviations of $-\Delta\gamma^{(\mathrm{mid})} \simeq 1$–$2\%$. The $\gamma^{(\mathrm{mid})}$ estimates are also listed in Table 6 and plotted in Figure 6.

5.4. Comparisons Between Tables

We single out the results of the 1-D radial model with $\gamma = 0.083$ and 0.039 (Table 6), and we compare them with the S_8 models listed in Tables 1 and 2. There is a general consensus in the following sense:

- The $\gamma = 0.039$ models indicate that the S_8 tension can only be resolved if the tidal activation redshift is enormous (typically $z_\star \approx 30$–12 for $S_8 \approx 0.76$–0.78). Unless S_8 turns out to be ≥ 0.79 (see Table 2), this γ amplitude is inadequate for $\gamma\Lambda$CDM.

 doi:10.20944/preprints202601.1031.v1

- The $\gamma = 0.083$ models consistently demonstrate that an exterior drag force resolves the tensions in S_8 and H_0, provided that the tidal activation redshift is $z_\star \leq 7$ (see also the 1-D radial Model C4 with $z_\star = 7$ in Table 6). Given the approximate nature of the 1-D radial model and the exact models listed in Table 1, this threshold may have to be revised lower, notably to $z_\star \simeq 3.5$–6.5 (see Models A3–A6 in Table 1). At any rate, the adopted estimate of $\gamma = 0.083$ is clearly the best choice for the benchmark $\gamma\Lambda$CDM model.

The agreement between the $\gamma = 0.083$ Models A2 and C4 (Tables 1 and 6, respectively) raises an important issue: in this work, ad-hoc modifications (γ terms) were introduced in both the kinematic description of the Hubble flow and the dynamical equations that determine the growth of linear density perturbations. Then, it is not entirely clear why these two, seemingly independent, arbitrary modifications produced very similar outcomes. We undertake this issue in Appendix A, where we show that the two independent modifications of the kinematics and the dynamics are consistent with one another.

6. Summary and Conclusions

6.1. Summary

This cosmological study can be summarized as follows:

(a) In Section 1, we reviewed the two foundational ΛCDM problems (CCP and DCP) and the two major observational tensions (H_0 and S_8), emphasizing the empirical $\gamma = 8.3\%$ difference in observations that motivates a unified late-time explanation within the new $\gamma\Lambda$CDM model.

(b) In Section 2, we introduced a late-time drag term in the Euler equation and derived the corresponding linear perturbation equations in the conformal Newtonian gauge (sub-horizon limit) on a flat FLRW ΛCDM background.

(c) In Section 3, we solved the modified growth equation and showed that the added friction can suppress late-time structure growth and lower the predicted clustering amplitude into the observed low-redshift range, thereby addressing the S_8 tension.

(d) In Section 4, we analyzed the associated $O(\gamma)$ background modifications implied by the same kinematical prescription, including its impact on standard late-time and present-day expansion diagnostics.

(e) In Section 5, we developed a simplified 1-D radial LOS model for the late-time tidal environment of nonlinear structures and used it to estimate both the accumulated LOS recession contribution and the implied drag amplitude $\gamma(a_\star)$, where $a_\star$ is the scale factor of the tidal activation epoch.

6.2. Conclusions

① S_8 Tension.—After activation, the drag force adds more friction to the linear growth equation of perturbations, suppressing late-time growth and lowering the predicted clustering amplitude [42–44]. The solutions presented in Section 3 demonstrate that the parameter range consistent with the kinematic H_0 interpretation simultaneously yields the required reduction of parameter S_8 in a $\gamma\Lambda$CDM background with a benchmark value of $\gamma = 8.3\%$.

② Hubble Tension.—The $\gamma\Lambda$CDM model provides a late-time mechanism that biases local CDL determinations of the Hubble flow through an additional LOS contribution sourced by a statistically isotropized tidal environment with nonzero mean value (Section 5) [44–46]. In this picture, the inferred expansion rate is shifted relative to the ΛCDM background in a manner controlled by the same parameter γ that enters the modified kinematics (cf. Equation (43)).

③ Density Coincidence Problem.—In $\gamma\Lambda$CDM, parameter γ modifies both the recent acceleration threshold and the matter–vacuum equality threshold [26,38]. For the benchmark case analyzed in Section 4.5, these thresholds occur at nearly the same redshift (cf. Equations (56) and (59)), so the "recent" coincidence underlying the DCP in standard ΛCDM is effectively absent in $\gamma\Lambda$CDM (Section 4.5.1).

④ Cosmological Constant Problem.—The present framework does not address the magnitude of the vacuum energy predicted by quantum field theory (cf. [47,48]). As in the standard ΛCDM, the Λ field is treated phenomenologically as an input to the background dynamics (Section 4). We do however find a scaled-down value $(1-2\gamma)\Lambda$ in $\gamma\Lambda$CDM , with the same scaling also modifying the dust-matter density field (cf. Equations (49) and (86)).

Author Contributions: Conceptualization, D.C. and D.K.; methodology, D.C. and S.L.; formal analysis, D.C.; investigation, D.C., D.K. and S.L.; resources, D.K. and S.L.; writing—original draft preparation, D.C.; writing—review and editing, D.K. and S.L.; project administration, D.K.; funding acquisition, S.L. All authors have read and agreed to the published version of the manuscript.

Funding: DMC and SGTL acknowledge support from NSF-AAG grant No. AST-2109004.

Data Availability Statement: No new data were created or analyzed in this study. The original contributions presented in this study are included in the article. Further inquiries can be directed to the corresponding author.

Acknowledgments: NASA, NSF, and LoCSST support over the years is gratefully acknowledged by the authors.

Conflicts of Interest: The authors declare no conflict of interest.

Abbreviations

The following abbreviations are used in this manuscript:

CCP	Cosmological Constant Problem
CDL	Cosmic Distance Ladder
CDM	Cold Dark Matter
CMB	Cosmic Microwave Background
DCP	Density Coincidence Problem
DES	Dark Energy Survey
EOS	Equation Of State
FEs	Friedmann Equations
FLRW	Friedman–Lemaître–Robertson–Walker
IVP	Initial Value Problem
KiDS	Kilo-Degree Survey
LOS	Line Of Sight
LSS	Large-Scale Structure
MVE	Matter–Vacuum Equality
ODE	Ordinary Differential Equation
RMS	Root Mean Square
SnIa	Supernovae of type Ia
TRGB	Tip of Red Giant Branch
1-D	One-Dimensional
3-D	Three-Dimensional

Appendix A. Reconciling Hubble-Flow Kinematics and Dynamics in $\gamma\Lambda$CDM

Appendix A.1. Modified Hubble-Flow Kinematics

In a purely kinematic model, the recession velocity of a target moving in an expanding FLRW background assumes the modified form

$$\mathbf{u}(t) \;=\; \big(1+\epsilon(t)\big)H(t)\,\mathbf{r}(t)\,, \tag{A1}$$

where the drag parameter $\epsilon(t) \ll 1$.

Differentiating with respect to cosmic time and using dot notation for the operator $\partial/\partial t$, we find to order $O(\epsilon)$ that

$$\dot{\mathbf{u}} \;=\; \Big[H\dot{\epsilon} \;+\; (1+\epsilon)\dot{H} \;+\; (1+2\epsilon)H^2\Big]\mathbf{r}\,. \tag{A2}$$

 doi:10.20944/preprints202601.1031.v1

Subtracting the conventional $\epsilon = 0$ terms $\dot{\mathbf{u}}_0 = (\dot{H} + H^2)\mathbf{r}$, we find to order $O(\epsilon)$ that the tidal part of the acceleration is

$$\dot{\mathbf{u}}^{(\mathrm{tid})} \;=\; \left[H\dot{\epsilon} \;+\; \epsilon\left(\dot{H} + 2H^2\right)\right]\mathbf{r}\,. \tag{A3}$$

Appendix A.2. Modified Hubble-Flow Dynamics

The recession velocity of a target in $\gamma\Lambda$CDM was assumed to take the modified form

$$\mathbf{u}(t,\mathbf{x}) \;=\; (1+\gamma)H(t)\mathbf{r}(t,\mathbf{x}) \;+\; \mathbf{v}(t,\mathbf{x})\,, \tag{A4}$$

where the drag parameter $\gamma \ll 1$ is a constant and the peculiar velocity $|\mathbf{v}| \ll H\mathbf{r}$.

The peculiar velocity field $\mathbf{v}$ is described by the linearized Euler equation modified to include a drag acceleration term of $O(\gamma)$, viz.

$$\dot{\mathbf{v}} \;+\; (1 + 2\gamma)H\mathbf{v} \;=\; -\frac{1}{a}\boldsymbol{\nabla}\Phi\,, \tag{A5}$$

where the del operator is taken in comoving coordinates $\mathbf{x}$, as in Section 2.2.2 of the main text.

Differentiating Equation (A4) with respect to cosmic time, we find that

$$\dot{\mathbf{u}} \;=\; (1 + \gamma)\dot{H}\mathbf{r} \;+\; (1 + \gamma)H\mathbf{u} \;+\; \dot{\mathbf{v}}\,, \tag{A6}$$

or, after some algebraic manipulations preserving only $O(\gamma)$ terms, that

$$\dot{\mathbf{u}} \;=\; \left(\dot{H} + H^2\right)\mathbf{r} \;+\; \left(H\,\mathbf{v} \;+\; \dot{\mathbf{v}}\right) \;+\; \gamma\left(\dot{H}\mathbf{r} + 2H^2\mathbf{r} + H\mathbf{v}\right). \tag{A7}$$

Using next Equation (A5) to replace the term $(H\,\mathbf{v} \;+\; \dot{\mathbf{v}})$ and subtracting finally the conventional $\gamma = 0$ terms $\dot{\mathbf{u}}_0 = (\dot{H} + H^2)\mathbf{r} \;-\; (\boldsymbol{\nabla}\Phi)/a$, we find to order $O(\gamma)$ that the tidal part of the acceleration is

$$\dot{\mathbf{u}}^{(\mathrm{tid})} \;=\; \gamma\left(\dot{H} + 2H^2\right)\mathbf{r} \;-\; \gamma H\mathbf{v}\,. \tag{A8}$$

The term $-\gamma H\mathbf{v}$ represents the drag exerted on the peculiar velocity field $\mathbf{v}$. Since $|\mathbf{v}| \ll H\mathbf{r}$, this term is of mixed higher order, viz. $O\big(\gamma|\mathbf{v}|/(H\mathbf{r})\big)$, and can subsequently be ignored. So, the tidal acceleration added to the Hubble expansion formally becomes

$$\dot{\mathbf{u}}^{(\mathrm{tid})} \;=\; \gamma\left(\dot{H} + 2H^2\right)\mathbf{r} \;+\; O(\gamma|\mathbf{v}|)\,. \tag{A9}$$

Appendix A.3. Linear First-Order ODE for the Drag Parameter $\epsilon(t)$

Comparing Equations (A3) and (A9), we find a linear first-order ODE for the time-dependent drag parameter $\epsilon(t)$ to $O(\gamma)$, viz.

$$\dot{\epsilon} \;+\; \frac{\dot{H} + 2H^2}{H}(\epsilon \;-\; \gamma) \;=\; 0\,. \tag{A10}$$

The fraction can be further simplified by introducing the deceleration parameter $q(t)$ defined by Equation (63) and a new independent variable

$$\zeta(t) \;\equiv\; \epsilon(t) \;-\; \gamma\,. \tag{A11}$$

Then, Equation (A10) takes the homogeneous form

$$\dot{\zeta} \;+\; (1 \;-\; q)H\,\zeta \;=\; 0\,. \tag{A12}$$

 doi:10.20944/preprints202601.1031.v1

The trivial solution of this ODE is $\zeta = 0$, which implies that

$$\epsilon(t) \;=\; \gamma\,. \tag{A13}$$

Thus, the kinematic drag parameter ϵ turns out to be independent of time and equal to constant γ. This is the desired mathematical result that we set out to derive in the first place (see Section 5.4), but it may not be the most interesting result in the realm of universal expansion. We discuss the general solution of Equation (A10) below.

Appendix A.4. General Solution of the Drag Parameter $\epsilon(t)$

Remarkably, the nontrivial solution of the ODE (A12) implies a time-dependent general solution $\epsilon(t)$ of the ODE (A10), viz.

$$\epsilon(t) \;=\; \gamma \;+\; \frac{CH_0}{a(t)^2 H(t)}\,, \tag{A14}$$

where CH_0 is the integration constant and C is a dimensionless constant.

We investigate the general case in which $C \neq 0$. The time-dependent part of $\epsilon(t)$, viz.

$$\Delta\epsilon(t) \;\equiv\; \frac{CH_0}{a(t)^2 H(t)}\,, \tag{A15}$$

although set to zero in $\gamma\Lambda$CDM, is physically very interesting for two reasons:

(1) In the matter-dominated ΛCDM, the product $a^2H(a)$ increases with cosmic time as $\sqrt{a\Omega_{\rm m0}}$, so $\Delta\epsilon(t)$ decays in time and $\epsilon(t) \to \gamma$ at late times. For example, considering the set of redshifts $z \in \{7, 10, 45, 100\}$, then $\Delta\epsilon(t)$ is diluted by factors of $\{5, 6, 12, 18\}$ between those epochs and the present, respectively. This dilution becomes much faster in the Λ-dominated future.

(2) The time-dependent term $\Delta\epsilon(t)$ can be written most transparently in conformal rather than cosmic time. In what follows, we recast Equation (A15) in conformal time η, thereby making its conformal properties explicit.

Appendix A.5. The Conformal Nature of $\Delta\epsilon(t)$

Conformal time η [26] is defined (up to an additive constant that we set to zero) by

$$\eta(t) \;\equiv\; \int_0^t \frac{d\tau}{a(\tau)}\,, \tag{A16}$$

so that

$$\frac{dt}{d\eta} \;=\; a(t)\,. \tag{A17}$$

In this convention, cosmic time $t \in [0, \infty)$ is mapped monotonically to $\eta \in [0, \eta_\infty]$, where η_∞ is the finite late-time limit in an eternally expanding matter+Λ universe.

Using the definition of the Hubble parameter $H(t) \equiv \dot{a}/a$, as well as prime notation for the operator $d/d\eta$, we recast Equation (A15) to its conformal form, viz.

$$\Delta\epsilon(\eta) \;=\; \frac{CH_0}{a'(\eta)}\,. \tag{A18}$$

Thus, the product $a'(\eta)\Delta\epsilon(\eta)$ is an invariant of the homogeneous ODE (A12) (that is, the ODE admits a first integral fixed by initial conditions). Furthermore, Equation (A18) shows that $\Delta\epsilon$ is naturally expressed in conformal time, since it is directly tied to the conformal-time expansion $a'(\eta) = a(\eta)\mathcal{H}(\eta)$ (with the conformal Hubble parameter defined by $\mathcal{H}(\eta) \equiv a'/a$), rather than to the cosmic-time rate $\dot{a}(t) = a(t)H(t)$.

 doi:10.20944/preprints202601.1031.v1

Then, in the matter-dominated and Λ-dominated epochs, we find that

$$a(\eta) \propto \eta^2 \quad \Longrightarrow \quad \Delta\epsilon(\eta) \propto \eta^{-1}, \tag{A19}$$

and

$$a(\eta) \propto (\eta_\infty - \eta)^{-1} \quad \Longrightarrow \quad \Delta\epsilon(\eta) \propto (\eta_\infty - \eta)^2, \tag{A20}$$

respectively. Thus, during matter domination, $\Delta\epsilon(\eta)$ decreases as a mild power law in conformal time, whereas in the Λ-dominated regime, it is driven rapidly to zero as $\eta \to \eta_\infty$, reflecting the asymptotic de Sitter scaling of the conformal expansion $\mathcal{H}(\eta) \propto (\eta_\infty - \eta)^{-1}$. (Here, $\mathcal{H}(\eta) \to \infty$ as $\eta \to \eta_\infty$, but the physical Hubble rate $H = \mathcal{H}/a$ tends to a finite constant, as $a \to \infty$ too.)

On the other hand, our present time lies in the transition regime of η, where the above limiting behaviors are not representative. For $a \to a_0 = 1$, it is easier to work with cosmic time $t \to t_0$ and Equation (A15), which takes the form

$$\Delta\epsilon(t_0) = C, \tag{A21}$$

which provides an initial condition that fixes the integration constant C of the solution of ODE (A12). Thus, in $\gamma\Lambda$CDM, we have effectively chosen to set $\Delta\epsilon(t_0) = 0$, in which case $\epsilon(t) = \gamma$ is constant at all times.

References

1. Planck Collaboration; Aghanim, N.; Akrami, Y.; Ashdown, M.; Aumont, J.; Baccigalupi, C.; Ballardini, M.; Banday, A.J.; Barreiro, R.B.; Bartolo, N.; et al. Planck 2018 results. VI. Cosmological parameters. *Astron. Astrophys.* **2020**, *641*, A6.
2. Alam, S.; Aubert, M.; Avila, S.; Balland, C.; Bautista, J.E.; Bershady, M.A.; Bizyaev, D.; Blanton, M.R.; Bolton, A.S.; Bovy, J.; et al. (eBOSS Collaboration). Completed SDSS-IV extended Baryon Oscillation Spectroscopic Survey: Cosmological implications from two decades of spectroscopic surveys at the Apache Point Observatory. *Phys. Rev. D* **2021**, *103*, 083533.
3. Einstein, A. Cosmological considerations in the general theory of relativity. *Sitzungsber. Preuss. Akad. Wiss. Phys. Math. Kl.* **1917**, 142.
4. Riess, A.G.; Filippenko, A.V.; Challis, P.; Clocchiatti, A.; Diercks, A.; Garnavich, P.M.; Gilliland, R.L.; Hogan, C.J.; Jha, S.; Kirshner, R.P.; et al. Observational Evidence from Supernovae for an Accelerating Universe and a Cosmological Constant. *Astron. J.* **1998**, *116*, 1009.
5. Perlmutter, S.; Aldering, G.; Goldhaber, G.; Knop, R.A.; Nugent, P.; Castro, P.G.; Deustua, S.; Fabbro, S.; Goobar, A.; Groom, D.E.; et al. Measurements of Ω and Λ from 42 High-Redshift Supernovae. *Astrophys. J.* **1999**, *517*, 565.
6. Shajib, A.J.; Frieman, J.A.; Scalar-field dark energy models: Current and forecast constraints. *Phys. Rev. D* **2025**, *112*, 063508.
7. Carroll, S.M. The Cosmological Constant. *Living Rev. Relativity* **2001**, *3*, 1.
8. Martin, J. Everything you always wanted to know about the cosmological constant problem (but were afraid to ask). *Comptes Rendus Physique* **2012**, *13*, 566.
9. Weinberg, S. The Cosmological Constant Problem. *Rev. Mod. Phys.* **1989**, *61*, 1.
10. Peebles, P.J.E. *Principles of Physical Cosmology*; Princeton University Press: Princeton, NJ, USA, 1993.
11. Ostriker, J.; Steinhardt, P. The observational case for a low-density Universe with a non-zero cosmological constant. *Nature* **1995**, *377*, 600.
12. Steinhardt, P.J. Cosmological implications of the end of inflation. *Phys. Rev. D* **1998**, *58*, 103512.
13. Verde, L.; Treu, T.; Riess, A.G. Tensions between the early and late Universe. *Nature Astronomy* **2019**, *3*, 891.
14. Di Valentino, E.; Mena, O.; Pan, S.; Visinelli, L.; Yang, W.; Melchiorri, A.; Mota, D.F.; Riess, A.G.; Silk, J. In the realm of the Hubble tension—a review of solutions. *Class. Quantum Grav.* **2021**, *38*, 153001.
15. Perivolaropoulos, L.; Skara, F. Challenges for ΛCDM: An update. *New Astron. Rev.* **2022**, *95*, 101659.
16. Riess, A.G.; Yuan, W.; Macri, L.M.; Scolnic, D.; Brout, D.; Casertano, S.; Jones, D.O.; Murakami, Y.; Anand, G.S.; Breuval, L.; et al. A Comprehensive Measurement of the Local Value of the Hubble Constant with 1

 doi:10.20944/preprints202601.1031.v1

km/s/Mpc Uncertainty from the Hubble Space Telescope and the SH0ES Team. *Astrophys. J. Lett.* **2022**, *934*, L7.
17. Freedman, W.L. Measurements of the Hubble Constant: Tensions in Perspective. *Astrophys. J.* **2021**, *919*, 16.
18. Asgari, M.; Lin, C.A.; Joachimi, B.; Giblin, B.; Heymans, C.; Hildebrandt, H.; Kannawadi, A.; Kuijken, K.; Wright, A.H.; Bilicki, M.; et al. (KiDS Collaboration). KiDS-1000 cosmology: Cosmic shear constraints and comparison between two point statistics. *Astron. Astrophys.* **2021**, *645*, A104.
19. Abbott, T.M.C.; Aguena, M.; Alarcon, A.; Allam, S.; Alves, O.; Amon, A.; Andrade-Oliveira, F.; Annis, J.; Avila, S.; Bacon, D.; et al. (DES Collaboration). Dark Energy Survey Year 3 results: Cosmological constraints from galaxy clustering and weak lensing. *Phys. Rev. D* **2022**, *105*, 023520.
20. Linder, E.V. Cosmic Growth History and Expansion History. *Phys. Rev. D* **2005**, *72*, 043529.
21. Poulin, V.; Smith, T.L.; Karwal, T.; Kamionkowski, M. Early Dark Energy can Resolve the Hubble Tension. *Phys. Rev. Lett.* **2019**, *122*, 221301.
22. Heisenberg, L. A systematic approach to generalisations of General Relativity and their cosmological implications. *Phys. Rep.* **2019**, *796*, 1.
23. Wang, B.; Abdalla, E.; Atrio-Barandela, F.; Pavón, D. Dark matter and dark energy interactions: theoretical challenges, cosmological implications and observational signatures. *Rep. Prog. Phys.* **2016**, *79*, 096901.
24. Hill, J.C.; McDonough, E.; Toomey, M.W.; Alexander, S. Early dark energy does not restore cosmological concordance. *Phys. Rev. D* **2020**, *102*, 043507.
25. Turner, M.S. Everyone wants something better than ΛCDM. *arXiv* **2025**, 2510.05483. https://arxiv.org/abs/2510.05483 (accessed on 1 January 2026)
26. Dodelson, S. *Modern Cosmology*; Academic Press: San Diego, CA, USA, 2003.
27. Jeans, J.H. I. The Stability of a Spherical Nebula. *Phil. Trans. Roy. Soc. London A*, **1902**, *199*, 1.
28. Peebles, P.J.E. *The Large-Scale Structure of the Universe*; Princeton University Press: Princeton, NJ, USA, 1980; pp. 48, 128, 391.
29. Ellis, G.F.R. The evolution of inhomogeneities in expanding Newtonian cosmologies. *Mon. Not. R. Astron. Soc.* **1990**, *243*, 509.
30. Jones, D.O.; Scolnic, D.M.; Foley, R.J.; Rest, A.; Kessler, R.; Challis, P.M.; Chambers, K.C.; Coulter, D.A.; Dettman, K.G.; Foley, M.M.; et al. The Foundation Supernova Survey: Measuring Cosmological Parameters with Supernovae from a Single Telescope. *Astrophys. J.* **2019**, *881*, 19.
31. Hawking, S.W.; Ellis, G.F.R. *The large scale structure of space-time*; Cambridge University Press: Cambridge, UK, 1973; p. 84.
32. Hildebrandt, H.; Viola, M.; Heymans, C.; Joudaki, S.; Kuijken, K.; Blake, C.; Erben, T.; Joachimi, B.; Klaes, D.; Miller, L. KiDS-450: cosmological parameter constraints from tomographic weak gravitational lensing. *Mon. Not. R. Astron. Soc.* **2017**, *465*, 1454.
33. Nesseris, S.; Sapone, D. Accuracy of the growth index in the presence of dark energy perturbations. *Phys. Rev. D* **2015**, *92*, 023013.
34. Hartman, P. *Ordinary Differential Equations*; Wiley: New York, NY, USA, 1964.
35. Christodoulou, D.M.; Katatbeh, Q.D. A powerful diagnostic tool of analytic solutions of ordinary second-order linear homogeneous differential equations. *Advances in Difference Equations* **2017**, *2018*, 208.
36. Shampine, L.F.; Reichelt, M.W. The MATLAB ODE Suite. *SIAM Journal on Scientific Computing* **1997**, 18, 1.
37. MathWorks. MATLAB Documentation, ode45 - Runge-Kutta (4,5) method for solving ODEs; https://www.mathworks.com/help/matlab/ref/ode45.html (accessed on 27 December 2025).
38. Ryden, B. *Introduction to Cosmology*, Second Edition; Cambridge University Press: New York, NY, USA, 2017; Sections 6.1 and 5.4.2.
39. Shibuya, T.; Ouchi, M.; Harikane, Y. Morphologies of ∼ 190,000 Galaxies at z = 0–10 Revealed with *HST* Data. I. Size Evolution. *Astrophys. J. Suppl. Series* **2015**, *219*, 15.
40. Oesch, P.A.; Bouwens, R.J.; Illingworth, G.D.; Labbé, I.; Stefanon, M. The Dearth of $z \sim 10$ Galaxies in All HST Legacy Fields—The Rapid Evolution of the Galaxy Population in the First 500 Myr. *Astrophys. J.* **2018**, *855*, 105.
41. Bradley, L.D.; Coe, D.; Brammer, G.; Furtak, L.J.; Larson, R.L.; Kokorev, V.; Andrade-Santos, F.; Bhatawdekar, R.; Bradač, M.; Broadhurst, T. High-redshift Galaxy Candidates at z = 9–10 as Revealed by JWST Observations of WHL0137-08. *Astrophys. J.* **2023**, *955*, 13.
42. Nguyen, N.-M.; Huterer, D.; Wen, Y. Evidence for Suppression of Structure Growth in the Concordance Cosmological Model. *Phys. Rev. Lett.* **2023**, *131*, 111001.

 doi:10.20944/preprints202601.1031.v1

43. Lin, M.-X.; Jain, B.; Raveri, M.; Baxter, E.J.; Chang, C.; Gatti, M.; Lee, S.; Muir, J. Late time modification of structure growth and the S_8 tension. *Phys. Rev. D* **2024**, *109*, 063523.
44. Poulin, V.; Bernal, J.L.; Kovetz, E.D.; Kamionkowski, M. Sigma-8 tension is a drag. *Phys. Rev. D* **2023**, *107*, 123538.
45. Weinberg, D.H.; Mortonson, M.J.; Eisenstein, D.J.; Hirata, C.; Riess, A.G.; Rozo, E. Observational Probes of Cosmic Acceleration. *Phys. Rep.* **2013**, *530*, 87.
46. Di Valentino, E.; Melchiorri, A.; Silvestri, A. Cosmology Intertwined: A Roadmap for the Hubble Tension. *Nat. Astron.* **2021**, *5*, 851.
47. Ryskin, G. Vanishing vacuum energy. *Astroparticle Phys.* **2020**, *115*, 102387.
48. Ryskin, G. The emergence of cosmic repulsion. *Astroparticle Phys.* **2015**, *62*, 258.